annual report 1985

nuclear physics laboratory
university of washington

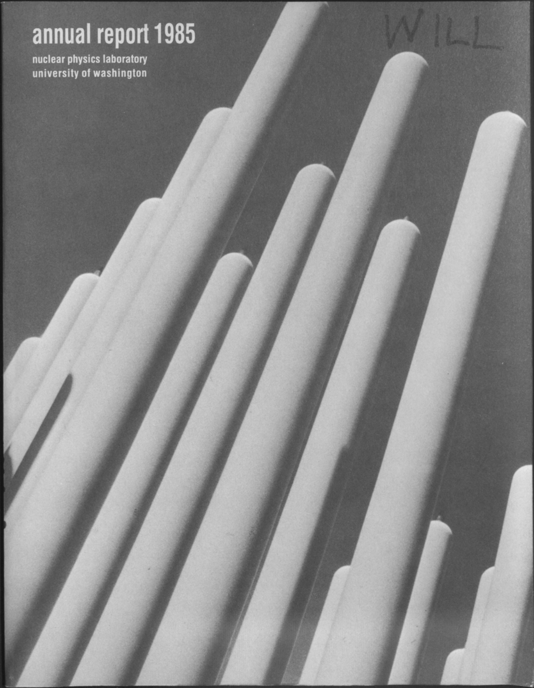

ANNUAL REPORT

Nuclear Physics Laboratory
University of Washington
April, 1985

Supported in part by the United States Department of Energy
under contract DE-AC06-81ER40048

This report was prepared as an account of work sponsored in part by the United States Government. Neither the United States nor the United States Department of Energy, nor any of their employees, makes any warranty, express or implied, or assumes any legal liability or responsibility for the accuracy, completeness or usefulness of any information, apparatus, product or process disclosed, or represents that its use would not infringe privately-owned rights.

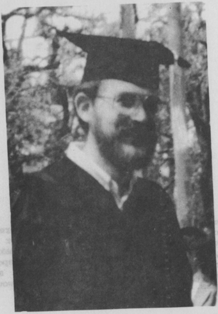

John L. Osborne
1948 to 1985

In Memory

John L. Osborne

John L. Osborne first came to the Nuclear Physics Laboratory as an University of Washington undergraduate physics major. He was eager to do a research project and joined Eric Adelberger and Kurt Snover in measuring the isospin violating particle widths of narrow T=2 states in ^{28}Si and ^{24}Mg. John made a big contribution to the experimental work and took over the analysis of the data. Two papers resulted from this work. In 1977, he graduated from the University of Washington with a B.S. in physics and mathematics with distinction in physics and began graduate study in physics at Caltech. He chose to work in nuclear astrophysics under Professor Charles Barnes. His thesis topic was a remeasurement of low energy cross section for the ^{3}He(α,γ) reaction. Experimental work by a German group had indicated that the accepted values for these cross sections were too low and that the celebrated "solar neutrino puzzle," was perhaps due to erroneous ^{3}He(α,γ) cross sections. John's thesis work decisively ruled out this possibility.

In July 1982, John arrived in Seattle to take up a postdoctoral position in the Nuclear Physics Laboratory. He worked with Eric Adelberger on several β decay measurements and on the ^{14}N parity mixing experiment, and with Kurt Snover on statistical γ-ray emission from heavy ion reactions.

In Seattle John experienced a recurrence of problems with a rare brain disorder that had first occurred in his graduate school days. The disease required delicate brain surgery. Unfortunately, the operation became necessary at shorter and shorter intervals and placed increasingly large strains on his system. However, throughout it all John retained his marvelous sense of humor. He never complained and was invariably cheerful. John continued his research work until just a few weeks before his death on March 21, 1985.

We will always remember John for his irrepressible and delightful spirit. One episode in particular symbolizes this. The Physical Review Letter article describing his thesis work ends with the sentence "We extend sincere thanks to Martin Weiss, M.D. for his expert repair of an important part of the apparatus." The apparatus of course was John himself.

INTRODUCTION

This Report summarizes all work during the year ending in April, 1985 done in the Nuclear Physics Laboratory or by our staff at other research institutions. Most staff projects are supported by the Laboratory's Department of Energy contract, two major projects are supported in part by the Murdock Charitable Trust, and outside users receive support from a variety of sources.

We are very pleased to note Eric Adelberger's selection as this year's recipient of the Tom W. Bonner prize in Nuclear Physics. The prize was awarded at the Spring Meeting of the A.P.S. He was cited "for his outstanding contributions in using nuclei to study fundamental symmetries, particularly studies of parity violation and isospin mixing...and especially the combination of breadth of physical insight and experimental skill manifested in this work." Congratulations, Eric.

The booster project continues to grow in intensity. The lead plating lab is in operation. A number of low-beta resonators have been plated and successfully tested at this Laboratory. Prototype support electronics for the resonators have performed well, and full production is now underway. The helium refrigerator is installed and has made liquid helium at performance levels considerably above specs. The level of activity remains very high, and new staff members have made a very stimulating addition to the Laboratory.

The new polarized ion source is almost finished. Most recently the cesium source has produced 15 mA of 40 keV beam. Following a four-hour operating period we noted that this beam had sputtered 500 mg of steel and 300 mg of copper from various jury-rigged assemblies! We are about to operate the system in full cross-beams mode.

We have completed a program to determine astrophysically significant cross sections for gamma ray production in alpha-particle-induced reactions. This survey complements earlier work on proton-induced reactions.

The shape of the giant dipole resonance (GDR) built on excited states in complex particle collisions reveals exciting new information on the properties of "hot" nuclei. We have observed a splitting of the GDR built on excited states in ^{160}Er and ^{166}Er which indicates that these nuclei have the same prolate deformation at moderate spin and temperature as is observed at low excitation energies. We see similar persistence of strong deformation in mass 70-90, and in several cases nuclei which are not strongly deformed in the ground state develop a distribution of deformation at finite temperature. In other work we note that γ-ray yields far in excess of those appropriate to statistical compound-nuclear decay and large forward-backward asymmetries near and above the GDR provide evidence of a nonstatistical reaction mechanism in ^{3}He- and alpha-induced reactions.

We have expanded our search for E2 (and higher) isovector resonances via the (γ,n) reaction. To date we see clear evidence for E2 isovector resonances in Pb at 23 MeV and Cd at 26 MeV. We have improved the neutron detector efficiency and carried out theoretical calculations of photo-neutron yields and asymmetries. Calculations which take into account E2 and E1 resonances with simple shapes do not reproduce our observations.

A study of sub-barrier fusion-fission has revealed broader spin distributions than can be accounted for in terms of known effects such as barrier penetration and barrier fluctuations due to nuclear deformation. We are attempting to characterize the orbiting complex in the $^{12}C+^{28}Si$ reaction by looking at the 4.43 MeV gammas from ^{12}C. The excited state population is less than expected on the basis of simple statistical and molecular models.

At higher bombarding energy we have been characterizing the mechanism for production of Z=3-7 fragments in 20 MeV/A ^{35}Cl-induced reactions. The energy correlation and separation energy spectra of coincident fragments are characteristic of sequential decay. We find no evidence for prompt fragmentation.

We continue to refine hardware for the ^{14}N nuclear parity mixing experiment. A major improvement has been incorporation of a system to move the target in a raster pattern so that target nonuniformity effects can be studied and eliminated. A computer and peripherals for an on-line data acquisition and experiment control system have recently been delivered. We eagerly await polarized beam from the new source, in order to pursue further development and final data acquisition.

We continue to refine the hydrogen atom solenoid. After much analysis we have a field measurement system good to $1/10^5$. A study of temperature effects shows that the solenoid creeps in a sort of caterpillar motion during heating and cooling, with attendant field distortion at the $5/10^5$ level. We now understand this effect and how to control it. This seems to be the final barrier to reproducibly shimming the solenoid to the $1/10^5$ level.

We have submitted for publication a long paper in which the relative sizes of many pion cross-sections are well accounted for in terms of a simple classical model. There remains, however, one striking disagreement between available data and the model. The data seem to indicate smaller ratios for corresponding π^- to π^+ cross-sections than one would reasonably expect. We intend to pursue this problem experimentally. In other work we have finished analyzing the data on relative pion scattering cross-sections in ^1H, ^2H, ^3He, and ^4He, and are in the course of interpreting these fairly precise data in terms of models which take into account the interplay between the π-nucleon scattering in these nuclei and pion absorption.

We have recently completed two pilot studies in accelerator-based radiocarbon dating. In one, the ages of biological samples from the dry valleys of Antarctica provide important clues to the climatic history of that region during the past 20,000 years. In the second, we seek to determine the sources of organic materials transported by the Amazon river to the ocean in order to understand the global CO_2 budget. In either case the amount of material available is 1000 times too small for conventional methods.

With great sadness we note the death of John Osborne, a good friend, a stimulating and amusing colleague.

We close this introduction with a reminder that the articles in this report describe work in progress and are not to be regarded as publications or quoted without permission of the investigators. In each article the names of the investigators have been listed alphabetically, but where appropriate the names of those primarily responsible for the report have been underlined.

As always, we welcome applications from outsiders for the use of our facilities. As a convenient reference for potential users, the table on the following page lists the vital statistics of our accelerators. For further information please write or telephone Dr. W.G. Weitkamp, Technical Director, Nuclear Physics Laboratory, University of Washington, Seattle, WA 98195; (206) 543-4080.

The editors thank Barbara Fulton for dealing with the many headaches of report production in the face of an already full work load, and Maria Ramirez for help keeping the figures straight.

Thomas A. Trainor
Scientific Editor

William G. Weitkamp
Technical Editor

TANDEM VAN DE GRAAFF ACCELERATOR

A High Voltage Engineering Corp. Model FN purchased in 1966 with NSF funds; operation funded primarily by the U.S. Department of Energy. See W.G. Weitkamp and F.H. Schmidt, "The University of Washington Three Stage Van de Graaff Accelerator," Nucl. Instrum. Meth. 122, 65 (1974).

Available Energy Analyzed Beams:

Ion	Max. Current (μA)	Max. Practical Energy (MeV)
p,d	20	18
polarized p,d	0.1	18
He	1.5	27
Li	0.2	36
C	1.8	63
N	0.2	62
O	1	72
Si	0.1	90
Cl	0.2	90
Ni	0.005	99
Br	0.05	108
Ag	0.001	108

60-INCH CYCLOTRON

A fixed energy cyclotron constructed in 1950-52 with State of Washington funds; operated with income from outside users. See F.H. Schmidt, G.W. Farwell, J.E. Henderson, T.J. Morgan, and J.F. Streib, "The University of Washington Sixty-Inch Cyclotron," Rev. Sci. Instrum. 25, 499 (1954).

Available Target Box Beams:

Ion	Maximum Current (μA)	Energy (MeV)
p	100	11
d	150	22
^{4}He	30	42

TABLE OF CONTENTS

1. ASTROPHYSICS AND COSMOLOGY

1.1 Alpha-Particle Cross Sections Relevant to Gamma-Ray Astronomy

D. Bodansky, P. Dyer,* D.D. Leach, E.B. Norman,† and A.G. Seamster+

The cross sections for the production of the most prominent gamma-ray lines from alpha-particle bombardment of ^{12}C, ^{14}N, and ^{16}O have been determined from threshold to E_α=27 MeV.[1] At these energies, the most strongly excited lines are those from (α,α') reactions, in contrast to the situation for incident protons[2] where above E_p=20 MeV the cross section for the production of the 4.439-MeV ^{12}C line from the (p,pα) reaction on ^{16}O exceeds any other p+^{12}C or p+^{16}O gamma-ray cross section, and also in contrast to α+^{56}Fe reactions,[3] where the strongest gamma-ray lines are those following emission of one or two nucleons from the compound nucleus, ^{60}Ni.

As reported previously,[1] the cross sections for the production of the the 4.439-MeV ^{12}C and 2.313-MeV ^{14}N lines are larger in (α,α') reactions than in (p,p') reactions. Similarly, for most energies above 14 MeV, the (α,α') cross section for the production of the 6.130-MeV ^{16}O line is more than twice as great as the (p,p') cross section. Measured data extend to E_p=23 MeV, where the cross section ratio is about 2.9. These results suggest that if gamma rays are produced primarily at low energies (less than a few tens of MeV per nucleon), alpha particles may play a significant role in astronomical sources despite their fluxes being lower than proton fluxes.

References:

* Los Alamos National Laboratory, Los Alamos, NM 87545.
† Present address: Lawrence Berkeley Laboratory, Berkeley, CA 94720.
\+ Present address: John Fluke Manufacturing Co., Everett, WA 98206.

1. Nuclear Physics Laboratory Annual Report, University of Washington (1984) p. 1.
2. P. Dyer, D. Bodansky, A.G. Seamster, E.B. Norman, and D.R. Maxson, Phys. Rev. C 23, 1865 (1981).
3. A.G. Seamster, E.B. Norman, D.D. Leach, P. Dyer, and D. Bodansky, Phys. Rev. C 29, 394 (1984).

******

1.2. Nucleosynthesis of $^{180}Ta^m$

S.E. Kellogg and E.B. Norman*

We continue to be interested in the nucleosynthetic mechanism responsible for the production of the naturally-occurring isomer $^{180}Ta^m$. Our investigation centers on the Beer and Ward[1] theory that $^{180}Ta^m$ can be produced in hot stellar environments by the standard s and/or r neutron capture processes through the fractional beta decay of $^{180}Hf^m$, f_β. As described in previous Annual Reports,[2] we have been looking for the 214 keV endpoint βdecay directly to $^{180}Ta^m$ by using a VETO technique to suppress the dominant conversion line spectrum and a software time delay to suppress the ^{181}Hf β continuum. We were able to obtain an early Oak Ridge batch of isotopically enriched $^{179}HfO_2$ uncontaminated with W and have developed methods of producing thin sources by dissolving the oxide in concentrated HF acid after n-activation. We remain bothered by the instability of our surface barrier detector in the presence of the HfF_4 source.

A paper has been published describing our observation of a weak 100.7 keV γ ray in the decay of $^{180}Hf^m$.[3] We have interpreted the new γ transition to be between the $J^\pi=8^+$ excited state and 9^- isomer in ^{180}Ta following the 2.3×10^{-4} β-decay branch from $^{180}Hf^m$. Takahashi[4] has performed bound-state β decay calculations which Beer and Macklin[5] have shown enhance the stellar production of $^{180}Ta^m$. Enhancement factors for nominal s-process conditions of 4.9 and 14.4 for the direct isomer to isomer and isomer to excited state β decays convert to limits on the s-process production of $^{180}Ta^m$ between 5% and 110%. In a second paper we have registered our reservations concerning the survivability of $^{180}Ta^m$ in a hot s-process environment where photodeexcitation and positron annihilation-deexcitation processes must be considered.[6]

The r-process can contribute to the nucleosynthesis of $^{180}Ta^m$ if some fraction f_m of the decay of $J^\pi=3^-$ ^{180}Lu (5.5 min) feeds $^{180}Hf^m$ (5.5 hr). Our limit of $f_m \leq 0.06\%$ was obtained by radiochemical separation of Lu from Hf following the $^{180}Hf(n,p)$ reaction.[2] But Eschner et al. have reported a value of $f_m=0.46\pm0.15\%$ which they obtained by online mass separation following bombardment of a W target with ^{136}Xe.[7] Such a discrepancy in experimental results might be explained if there exists a high-spin, short-lived isomer of ^{180}Lu. Likely J^π candidates are 8^+ and 9^- (structurally identical to the low-lying high-spin states in ^{180}Ta) and recent calculations indicate that these two levels should lie within 200 keV of the 3^- ground state.[8] We have begun a series of experiments at the U of W Tandem and the Berkeley 88" Cyclotron designed to produce and directly observe the decay of a ^{180}Lu isomer with a 5 sec to 1 minute halflife. The energies of these high-spin states are low enough that a substantial fraction of the ^{180}Lu may be thermally equilibrated and then trapped in the isomeric state during the cooling-off period following a supernova explosion. We are driven to carefully consider this more complicated model-dependent scenario because the $^{180}Ta^m$ ultimately produced in the r-process does not have to endure the high temperature conditions which s-process-produced ^{180}Ta must.

References:

* Lawrence Berkeley Laboratory, Berkeley, CA 94720.

1. H. Beer and R. Ward, Nature 291, 308 (1981).
2. Nuclear Physics Laboratory Annual Report, University of Washington (1983) p. 1; ibid. (1984) p. 3.
3. S. Kellogg and E. Norman, Phys. Rev. C 31, 1505 (1985).
4. K. Takahashi, private communication.
5. H. Beer and R. Macklin, Phys. Rev. C 26, 1404 (1982).
6. E. Norman et al., Astrophys. J. 281, 360 (1984).
7. W. Eschner et al., Z. Phys. A 317, 281 (1984).
8. R. Hoff, private communication.

******

1.3 Equilibration of $^{176}Lu^{g,m}$ During the s-Process

T. Bertram, S.E. Kellogg, and E.B. Norman*

A paper describing our earlier photoactivation work has been accepted for publication.[1,2] As a result of photoexcitation and positron annihilation-excitation of the long-lived ground state of ^{176}Lu, it is concluded that $^{176}Lu^{g}$ and $^{176}Lu^{m}$ are in thermal equilibrium at the standard s-process temperature of 3.5×10^{8} K. This implies that $^{176}Lu^{g,m}$ is not a reliable s-process chronometer.

References:

* Lawrence Berkeley Laboratory, Berkeley, CA 97420.

1. Nuclear Physics Laboratory Annual Report, University of Washington (1983) p. 2; ibid. (1984) p. 3.
2. E. Norman, et al., Astrophys. J. 291, 834 (1985).

2. NUCLEAR STRUCTURE

2.1 A Study of the Resonances in ^{14}N via the Reaction $^{13}C(p,\gamma)$

E.G. Adelberger, P.B. Fernandez, C.A. Gossett, J.L. Osborne, and V.J. Zeps

We are using the $0^+,0^-;I=1$ doublet in ^{14}N to study the $\Delta I=0$ part of the parity non-conserving (PNC) nucleon-nucleon interaction.[1] The $\langle 0^+|H_{pnc}|0^-\rangle$ PNC matrix element can only be determined from A_L if the widths and energies of the $0^+,0^-;I=1$ levels are accurately known.[2] We studied the $^{13}C(p,\gamma)$ reaction to obtain these values.

We used the FN tandem to produce a proton beam with energies from 495 keV to 3 MeV. Gammas were detected simultaneously in the 25.4 cm x 25.4 cm NaI spectrometer and a large PGT Ge(Li) detector, each at 90^o with respect to the beam axis. Detection efficiencies for the NaI were determined from "tagged" photons from the $^{12,13}C(^3He,p\gamma)$ reactions.[3] The Ge(Li) efficiency was then normalized to the NaI γ_o-yield. Energy calibration was determined using the E_p=992 keV and 1382 keV $^{27}Al(p,\gamma)$ resonances and the E_p=1748 keV $^{13}C(p,\gamma)$ resonance.

For the $0^+;1$ width measurement, we fitted an excitation function for cascade transitions, thus suppressing the intense γ_o background from the $0^-;1$ resonance. We determined the target thickness to be (23.4±1) $\mu gm/cm^2$ from a fit to the narrow (~ 70 eV) E_p=1748 keV $2^+;1$ resonance. Both resonances were fitted using a program that incorporates the effects of beam energy spread and the discrete nature of energy loss in the target.[4] The width of the 0^+ state was determined to be $\Gamma_{0^+}^{cm}$ = (3.8±0.3) keV (see Fig. 2.1-1).

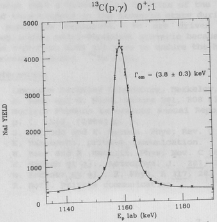

Fig. 2.1-1 Yield of cascade γ-rays over the $0^+;1$ resonance. The smooth curve is calculated for $\Gamma_{0^+}^{cm}$ = (3.8±0.3) keV This width is much narrower than the previously accepted value[5] $\Gamma_{0^+}^{cm}$ = (7±1) keV.

The $0^-;1$ width was obtained by measuring the γ_0 excitation function over the interval E_p=495 keV to 3 MeV using a 75 μgm/cm^2 target. This was done to correctly account for the tail of the strong $1^-;1$ resonance on which the $0^-;1$ lies. We fit the spectrum up to 2100 keV using a program that assumes 6 non-interfering Breit-Wigner resonances folded with target thickness (see Fig. 2.1-2). The widths, strengths, and energies were varied to minimize χ^2. Preliminary results give $\Gamma_{0^-}^{cm}$=(420±8) keV. We also determined the energy separation between the two 0^- levels to be ΔE=(157±5) keV. These values differ substantially from the accepted values[5] and lead to a larger enhancement of A_L for the PNC experiment, making ^{14}N an even more sensitive system for measuring the ΔI=0 PNC NN interaction.

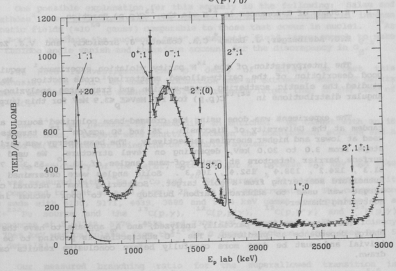

Fig. 2.1-2 γ_0 yield in the region of the $0^-;1$ resonance. By fitting the region 495 keV<E_p≤2200 keV, we determined $\Gamma_{0^-}^{cm}$ = (420±8) keV. Note the previously unobserved γ_0 decay of the E_p=2319 keV $1^+;0$ state.

From partially analyzed data, we see evidence for previously unobserved transitions, namely 9.39(2^-;0) → 5.83(3^-;0), 9.07(1^+;0) → 0.0(1^+;0), and 9.07(1^+;0) → 2.31(0^+;1). Complete analysis will give results concerning widths, strengths and energies of all isotropic γ-resonances in this region.

References:

1. Nuclear Physics Laboratory Annual Report, University of Washington (1984) p. 36.
2. E.G. Adelberger et al., Phys. Rev. C 30, 456 (1984).
3. Nuclear Physics Laboratory Annual Report, University of Washington (1985) p. 78.
4. E.G.Adelberger et al., Phys. Rev. C 15, 484 (1977).
5. F. Ajzenberg-Selove, Nucl. Phys. A 360, 1 (1981).

******

2.2 A Study of Resonances in ^{14}N via the $^{13}C(\vec{p},p)$ Reaction

E.G. Adelberger, J. Dahm,* C.A. Gossett, J. Sromicki,† and V.J. Zeps

The interpretation of the ^{14}N parity violation experiment[1] requires a good description of the parity-allowed scattering cross section. We have studied the elastic scattering cross-section and transverse analyzing-power angular distributions in $^{12,13}C(\vec{p},p)$ for 1.0 MeV$\leq E_p \leq$3.9 MeV for this purpose.

The experiment was done using the crossed-beam polarized source and EN tandem at the University of Wisconsin. 25 and 50 μgm/cm^2 ^{13}C targets were used at lower and higher energies respectively. The beam energy was varied in steps from 3.0 to 30.0 keV, depending on level structure. We used eight surface barrier detectors at center-of-mass angles of 39.4°, 55.3°, 70.9°, 91.3°, 124.2°, 138.4°, 152.4°, 166.3°. Solid angles were determined using Rutherford scattering from a gold target. Scattering from a natural carbon target was used to subtract carbon buildup due to poor vacuum in the scattering chamber.

The data have been partially analyzed, and A_T appears to have the same energy dependence as predicted. The ^{12}C subtraction is proving to be non-trivial and must be done more carefully before conclusive results can be drawn.

We would like to thank W. Haeberli† and P. Quin† for their generous help in making this experiment possible.

References:

* Department of Physics, University of Washington.
† Department of Physics, University of Wisconsin, Madison, WI 53706.
1. Nuclear Physics Laboratory Annual Report, University of Washington (1984) p. 36.

******

2.3 Does the Cabibbo Angle Vanish in Fermi Matrix Elements of High J States?

E.G. Adelberger, P.B. Fernandez, C.A. Gossett, J.L. Osborne, and V.J. Zeps

The CVC hypothesis and Cabibbo universality predict the same vector coupling constant G_{β}^{V} for all isospin analog transitions. But for the analog transition $^{35}Ar(3/2^{+}) \rightarrow {}^{35}Cl(3/2^{+})$ the measured[1] vector coupling constant is 3% greater than the value inferred from the $0^{+} \rightarrow 0^{+}$ transitions.

One possible explanation for this anomaly is the following: Salam and Strathdee[2] have predicted that the Cabbibo angle should vanish in intense magnetic fields ($\approx 10^{16}$ gauss) comparable to those that occur in nuclei. ^{35}Ar has J=3/2: perhaps the nucleons "see" a magnetic field large enough to make the Cabibbo angle vanish and therefore account for the discrepancy in G_{β}^{V}.[3]

We have reinvestigated the β^{+} decay of $^{24}Al(4^{+})$ to test this hypothesis. The $^{24}Al \rightarrow {}^{24}Mg$ analog transition has an extremely small GT matrix element and the magnetic moments involved are much larger than in the case of $^{35}Ar \rightarrow {}^{35}Cl$.

The ^{24}Al was produced by bombarding an enriched ^{24}Mg target with an 18 MeV proton beam. Targets were shuttled between the bombardment station and a shielded Ge(Li) detector using the UW 'rabbit' system.

The efficiency of the Ge(Li) detector for E_{γ} between 570 keV and 3548 keV was measured with ^{24}Na, ^{56}Co and ^{207}Bi sources.[4] At higher energies, it was compared to that of a 25.4 cm × 25.4 cm NaI spectrometer. The comparison was made with 6130, 9171, 4439, 3685 and 5284 keV gamma rays produced by a ^{13}C+^{238}Pu source and the $^{13}C(p,\gamma)$, $^{12}C(p,p'\gamma)$, $^{13}C(p,p'\gamma)$ and $^{15}N(p,\gamma)$ resonances at E_p=1748, 5370, 4525 and 7300 keV respectively. The efficiency at 7069 keV was calculated from the ^{24}Al β decay spectrum itself (see Ref. 5 for details).

Our measured branching ratio for the superallowed transition is (37.7±0.4)%. We combined it with the two most precise existing results[5,6] to obtain (37.9±0.4)%. We also measured the $^{24}Al(4^{+})$ lifetime by the multiscaling technique. Our result, $t_{1/2}$=(2.054±0.008) sec, agrees with the most recent measurement[7] of $t_{1/2}$=(2.054±0.009) sec. We combine these two results to obtain $t_{1/2}$=(2.054±0.006) sec. Including all corrections, we get a $ft_{1/2}$ value of (3130±41) sec. Taking into account the axial vector contribution to the rate, we obtain G_{β}^{V}=(1.4021±0.0093)×10^{-49} erg cm^{3}. This is in good agreement with G_{β}^{V}=(1.4130±0.0004)×10^{-49} erg cm^{3} inferred from the $0^{+} \rightarrow 0^{+}$ transitions. We conclude that the anomaly in ^{35}Ar must be due to some unidentified error, presumably in the determination of the axial vector contribution to the decay.

References:

1. E. Hagberg et al., Nucl. Phys. A 313, 276 (1979).
2. A. Salam and J. Strathdee, Nature 252, 569 (1974); Nucl. Phys. B 90, 203 (1975).
3. J.C. Hardy and I.S. Towner, Phys. Lett. B 58, 261 (1975).
4. Y. Yoshizawa et al., Nucl. Instrum. Meth. 174, 109 (1980) for E_γ<2700 keV; M. Hautala et al., Nucl. Instrum. Meth. 150, 594 (1979) for E_γ>2700 keV.
5. E.K. Warburton et al., Phys. Rev. C 23, 1242 (1981).
6. J. Honkanen et al., Physica Scripta 19, 239 (1979).
7. D.R. Goosman et al., Phys. Rev. C 4, 1800 (1971).

3. GIANT RESONANCES

3.1 Deformation of Heated Nuclei in the Rare Earth Region

J.A. Behr, G. Feldman, C.A. Gossett, J.L. Osborne, and K.A. Snover

Although a great deal of work has recently been focussed on the high spin properties of "cold" nuclei near the yrast line, very little is known about the properties of nuclei, particularly nuclear deformation, at elevated temperature. In analogy with the splitting of the Giant Dipole Resonance (GDR) in ground-state photoabsorption studies of deformed rare-earth nuclei, study of the shape of the GDR built on excited states in "hot" nuclei provides a means of investigating nuclear deformation at high excitation. We have observed[1] a splitting of the GDR built on excited states in the continuum γ spectra from the decays of $^{160}Er^*$ and $^{166}Er^*$ formed in $^{12}C+^{148}Sm$ and $^{12}C+^{154}Sm$ reactions, respectively. The observed shape of the GDR indicates that these highly excited Er nuclei have the same prolate deformation at elevated temperature, $T \sim 1.2$ MeV and moderate spin, $I \sim 0$–$25\ \hbar$ as deduced at low excitation from measurements of the quadrupole moment. We have also studied the decays of $^{156}Er^*$ formed in the $^{12}C+^{144}Sm$ reaction. While the ground state of ^{156}Er is not strongly deformed, the observed shape of the GDR built on excited states suggests that there is a distribution of finite deformation for the ensemble of excited nuclear states populated by the γ decay.

Gamma rays from the decays of $^{166}Er^*$, $^{160}Er^*$, and $^{156}Er^*$ were detected in an anticoincidence shielded 25.4 cm × 25.4 cm NaI detector. Pulsed beam and time-of-flight techniques were used to separate prompt γ rays produced in the target from other sources of background. The γ-ray spectra shown in the left portion of Fig. 3.1 exhibit two characteristic features of compound-nuclear statistical decay: a steeply falling low energy portion ($E_\gamma < 8$ MeV) due to γ decay following particle evaporation, and a high energy portion ($E_\gamma >$ 10 MeV) containing a "bump" near the GDR energy and arising from γ emission in direct competition with particle evaporation. The spectra were fitted from E_γ=9 to 21 MeV with a modified version of the statistical evaporation code CASCADE in which either a one- or two-component Lorentzian form (dashed and solid curves, respectively) was assumed for the GDR strength function. In the right portion of the figure the data and calculated curves have been multiplied by the factor $\exp(\alpha E_\gamma)$ in order to allow a more clear comparision of the experiment with theory.

For decays of $^{166}Er^*$ and $^{160}Er^*$ the single component fits are clearly inadequate while the two-component fits reproduce the spectral shapes well. The shape of the GDR built on highly excited states in these nuclei inferred from our best fits, in particular the mean resonance energy, total strength as well as the ratio of the strengths and the ratio of the widths for the two components, are remarkably similar to GDR shapes observed in ground-state photoabsorption studies of rare-earth nuclei of comparable deformation (for detailed results, see Ref. 1). The relative strengths of the two components indicate prolate deformation and the magnitude of the deformation deduced from the energy splitting is $\delta \sim 0.30$ and 0.25 for decays of $^{166}Er^*$ and $^{160}Er^*$, respectively. In the case of $^{156}Er^*$, the observed shape of the GDR is more broad than would be expected based on the ground-state deformation, which suggests that the ensemble of excited states populated by the γ decay contains a distribution of deformation.

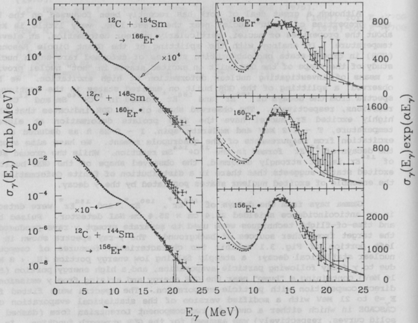

Figure 3.1 Left: Gamma-ray spectra from the decays of $^{166}Er^*$ (E_x=49.2 MeV), $^{160}Er^*$(43.2), and $^{156}Er^*$(42.4) formed in the $^{12}C + ^{154}Sm$, $^{12}C + ^{148}Sm$, and $^{12}C + ^{144}Sm$ reactions at E(^{12}C)=61.2, 61.2, and 65.5 MeV, respectively. Dashed and solid curves: CASCADE fits assuming a one- or two-component GDR, respectively (see text). Right: The product $\sigma_\gamma(E_\gamma)\exp(\alpha E_\gamma)$, where α^{-1}=1.45 for $^{166}Er^*$ and 1.40 MeV for $^{160}Er^*$ and $^{156}Er^*$.

Reference:

1. C.A. Gossett, K.A. Snover, J.A. Behr, G. Feldman, and J.L. Osborne, Phy. Rev. Lett. 54, 1486 (1985).

******

3.2 Statistical Decay of the Giant Dipole Resonance for Nuclei Near Z=50

J.A. Behr, G. Feldman, C.A. Gossett, J.H. Gundlach, T. Murakami, and K.A. Snover

To complement our studies of the Giant Dipole Resonance (GDR) built on excited states in nuclei with strong ground-state deformation (see Sec. 3.1) with studies of the GDR for nuclei with spherical or not strongly deformed shapes, we have begun a study of several nuclei in the region of the closed proton shell at Z=50. Ground-state photoabsorption studies of the tin isotopes from mass 116 to 124 confirm that these nuclei are relatively spherical at low excitation and that the shape of the GDR is reasonably well reproduced by a single-component Lorentzian form.

We have measured continuum γ-ray spectra from decays of $^{108}Sn^*$, $^{116}Sn^*$, and $^{115}Sb^*$ formed at initial excitation energies of 44.4, 54.8, and 54.2 MeV in the $^{16}O+^{92}Mo$, $^{18}O+^{98}Mo$, $^{12}C+^{103}Rh$ reactions, respectively. Preliminary analysis of the spectral shapes indicates that the GDR built on excited states in these nuclei is broader than expected from ground-state photoabsorption studies and that the shape of the GDR is not adequately described by a single-component resonance form. We also find that the GDR in $^{116}Sn^*$ is broader than that in $^{108}Sn^*$. The reason that the shape of the GDR of highly excited nuclei in this mass region is broader than would be expected based on ground-state studies, but not as clearly split as in the case of the strongly deformed Er nuclei (Sec. 3.1), may be that at moderate excitation the ensemble of nuclear states populated by the γ decay contains a distribution of deformation. Indeed, at zero temperature, calculated potential energy surfaces for these nuclei, as a function of β and γ deformation, have minima which are substantially more shallow than those for strongly deformed nuclei in the rare-earth region. Consideration of the effect of averaging over a distribution of deformed shapes may be required in order to fully understand the GDR shapes for nuclei at moderate temperature and spin which are not strongly deformed at low excitation energies.

In order to pursue the idea that the shape of the GDR depends on temperature, we have measured γ-ray spectral shapes from decays of $^{116}Sn^*$ formed at E_x(initial)=47.8, 54.8, and 66.6 MeV in the $^{18}O+^{98}Mo$ reaction for $E(^{18}O)$=53.5, 61.8, and 75.8 MeV, respectively. The nuclear temperatures corresponding to the mean final state energy populated by the γ decay in the three measurements are approximately 1.4, 1.5, and 1.7 MeV. Analysis of these results is currently in progress.

We have also measured the angular distribution for decays of $^{115}Sb^*$ formed at E_x(initial)=54.2 MeV in the $^{12}C+^{103}Rh$ reaction for $E(^{12}C)$=61.7 MeV. The purpose of this measurement is twofold; 1) to look for a possible asymmetry about $\theta=90^\circ$, which would be evidence for nonstatistical reaction contributions, and 2) to look for a dependence of the a_2 coefficient on E_γ in the region of the GDR bump, as would be expected for deformation splitting of the GDR. After accounting for the effect of the center-of-mass to laboratory transformation, there is no 90° asymmetry present within errors. However, the a_2 coefficient is small but nonzero, ~ -0.05 to -0.10, on the low side of the

GDR, E_γ ~ 10–15 MeV, and zero or perhaps positive on the high side of the GDR. We have observed similar results for the a_2 coefficient in the $^{12}C+^{154}Sm$ reaction for $E(^{12}C)$=61.5 MeV. While our measurements are consistent with the signs of a_2 expected for the upper and lower components of a split GDR due to prolate deformation, the observed magnitudes are so small that considerably more work is necessary to determine if the observed effects are indeed due to deformation.

******

3.3 Excited-State Giant Dipole Resonances in the $^{39}K(p,\gamma)^{40}Ca$ and the $^{40}Ca(p,\gamma)^{41}Sc$ Reactions

D.H. Dowell,* C.A. Gossett, L. Ricken,* A.M. Sandorfi,* and K.A. Snover

In last year's Annual Report,[1] we presented examples of spectra from the $^{39}K(p,\gamma)^{40}Ca$ and $^{40}Ca(p,\gamma)^{41}Sc$ reactions measured from E_p=10 to 36 MeV at Brookhaven National Laboratory. These spectra are highly structured, with pronounced, separated peaks corresponding to the strong, single-particle states in ^{41}Sc and the 1 particle-1 hole states in ^{40}Ca which are made strongly in proton stripping reactions. The discrete part of these spectra corresponding to final-state energy E_x^f<10 MeV in ^{40}Ca and <6 MeV in ^{41}Sc has now been analyzed by lineshape fitting, and the results[2] are shown in Fig. 3.3. On the left side of Fig. 3.3 are the measured excitation functions for the θ_γ=90° cross section derived from the lineshape fits to the spectra. The various transitions all show resonance behavior which peaks at progressively higher proton bombarding energy for transitions to higher energy final states. When the excitation curves are plotted as a function of gamma-ray energy $E_\gamma=E_p^{c.m.}+Q-E_x^f$, as shown in Fig. 3.3, the resonances line up at roughly $E_\gamma\cong$19 MeV, the energy of the ground state GDR. In some cases the resonances in the $^{39}K(p,\gamma)^{40}Ca$ reaction corresponding to E_x^f between 7 and 10 MeV appear to peak 1-2 MeV lower in γ-ray energy. This may be connected with isospin splitting since the strong $(1f2p)-1d_{3/2}^{-1}$ p-h states in this energy region are mostly T=1. The GDR built on these states should be a mixture of T=0 and T=2 components; thus the (p,γ) reaction, which picks out the lower isospin component, should peak at a lower γ-ray energy than for the T=1 GDRs built on the predominantly T=0 p-h final states at E_x^f below 7 MeV.

The (p,γ) excitation curves were fitted with a Lorentzian resonance shape, as shown in Fig. 3.3. The resonance widths Γ and integrated resonance strengths $(2J+1)\int\sigma(\gamma,p_o)dE$ derived from these fits are shown on the right side of Fig. 3.3. The resonance widths for the $^{39}K(p,\gamma)^{40}Ca$ resonances increase substantially over the range of final states studied, while the

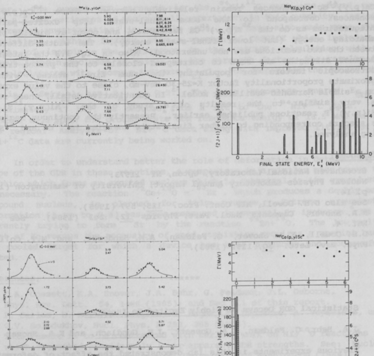

Fig. 3.3 Left side: Measured excitation functions and fitted curves for the $^{39}K(p,\gamma)^{40}Ca$ and $^{40}Ca(p,\gamma)^{41}Sc$ reaction. In each box, the final-state excitation energy is indicated. Right side: Resonance widths (points in top part of each figure section) and integrated strengths (solid bars) determined from the fitted excitation curves. The open and hatched bars are experimental values for $\Sigma(2J+1)C^2S$ taken from transfer reaction studies.

$^{40}Ca(p,\gamma)^{41}Sc$ resonances remain relatively narrow. These $^{40}Ca(p,\gamma)^{41}Sc$ resonances correspond to the same final-state 1f2p excited-particle configurations as do the $^{39}K(p,\gamma)^{40}Ca$ resonances, and occur at similar proton bombarding energy (but lower final-state energy). The width differences between the two reactions are not understood. Also in Fig. 3.3 the integrated resonance strengths are seen to correspond closely to the proton-transfer spectroscopic factors for populating the same final states, with an approximate proportionality factor K=25-30 MeV-mb, close to the value expected from a simple harmonic oscillator model.[3] In quantitative detail, these result are very similar to the results of a study of the $^{27}Al(p,\gamma)^{28}Si$ and $^{28}Si(p,\gamma)^{29}P$ reactions published earlier.[4] Presently the continuum region of the spectra corresponding to higher final-state energies in ^{40}Ca and ^{41}Sc is being analyzed.

References:

* Brookhaven National Laboratory, Upton, NY 11973.

1. Nuclear Physics Laboratory Annual Report, University of Washington (1984) p. 14.
2. See also D.H. Dowell, AIP Conf. Proc. 125, 597 (1985).
3. K.A. Snover, Comments Nucl. Part. Physics 12, 243 (1984). See also Ref. 4.
4. D.H. Dowell, K.A. Snover, G. Feldman, A.M. Sandorfi, and M.T. Collins, Phys. Rev. Lett. 50, 1191 (1983).

******

3.4 Statistical GDR Decays of Highly Excited Se Isotopes

J.A. Behr, G. Feldman, C.A. Gossett, J.H. Gundlach, and K.A. Snover

Previous experiments in this lab demonstrated the effect of deformation in highly excited nuclei in the rare earth region by observation of a splitting into two components of the giant dipole resonance built on highly excited states.[1] The purpose of the present work is to search for similar deformation effects for excited nuclei in the mass region of A=70-90. Some of these nuclei appear to be deformed; for example ground-state (γ,n) GDR studies for ^{76}Se suggest a split GDR. It is reasonable to expect that deformation may still be important in these nuclei at energies of E_x=30-40 MeV and possibly observable as a split GDR. The two GDR components are expected to be close together and overlapping so that good statistics are required, especially in the high-energy tail of the γ-ray spectrum, in order to extract reliable results by fitting the data with the statistical code CASCADE.

We have measured $^{64}Ni+^{12}C \rightarrow {}^{76}Se^*$ and $^{60}Ni+^{12}C \rightarrow {}^{72}Se^*$ at a bombarding energy of $E(^{12}C)$=45 MeV. Non-linear least squares fitting of the statistical model calculation to the data was performed with both a one-component and a two-component GDR. Preliminary calculations indicate that a one-component fit to the $^{64}Ni+^{12}C$ data gives poor results, while a two-component fit is much better. The summed GDR strength in the $^{64}Ni+^{12}C$ case was found to be $S_{E1}\approx 0.8$.[3] Our estimates of the overall uncertainty in this quantity, including measurement uncertainties, is roughly ±20%. We have also made some single calculations, without fitting, with a version of CASCADE which includes the effects of isospin. The difference in the CASCADE calculation with and without isospin included is mainly in the strength factor; the results from the calculations with isospin indicate $S_{E1}\approx 1$. For comparison the ground state GDR in $^{76}Se(\gamma,n)$ has $S_{E1} \sim 0.9$.[2] The mean resonance energy E_{GDR} is approximately 17 MeV, as deduced from a fit to the $^{64}Ni+^{12}C$ data. This compares well with the ground state GDR resonance energy of 16.5 MeV in this mass region.[2] Analysis of $^{60}Ni+^{12}C$ data along with improved fitting of the $^{64}Ni+^{12}C$ data are currently being worked on.

In order to understand better the role of deformation in determining the shape of the GDR in these reactions, a comparison in a similar mass range to a reaction which forms an excited nucleus which is spherical in its ground state is necessary. The reaction $^{72}Ge+^{18}O \rightarrow {}^{90}Zr^*$, which produces a doubly magic compound nucleus, is planned for this purpose. Extreme ground-state deformation (δ up to 0.4) has been measured in several Sr isotopes.[4] We are currently trying to form $^{80}Sr^*$ by the reaction $^{64}Zn+^{16}O$. The low melting point of Zn versus the necessity of good statistics requires a special backed and cooled target for which a device has been produced and successfully tested.

References:

1. C.A. Gossett, K.A. Snover, J.A. Behr, G. Feldman, J.L. Osborne, Phys. Rev. Lett. 54, 1486 (1985); and Sec 3.1 of this report.
2. P. Carlos, H. Beil, R. Bergere, J. Fagot, A. Lepretre, A. Veyssiere, and G.V. Solodukhov, Nucl. Phys. A 258, 365 (1975).
3. This result is to be contrasted with earlier work on $Ni+^{16}O$ reactions which suggested considerably lower apparent GDR strengths. See: Nuclear Physics Laboratory Annual Report, University of Washington (1984), Sec. 3.4.
4. C.J. Lister, B.J. Varley, H.G. Price, and J.W. Olness, Phys. Rev. Lett. 49, 308 (1982).

******

3.5 High Energy Nonstatistical γ-rays from ^{3}He- and α-Induced Reactions

J.A. Behr, G. Feldman, C.A. Gossett, J.H. Gundlach, and K.A. Snover

We measure inclusive γ-ray spectra with our NaI spectrometer, using time of flight to eliminate neutron events, comparing γ yields from ^{3}He- and α-induced reactions. In contrast to reactions induced by heavier projectiles (see Secs. 3.1, 3.2, 3.4), these reactions produce large yields of γ rays in the giant dipole resonance region (on targets with A>60) which cannot be explained by statistical decays from a compound nucleus. Angular distributions from the reactions 27 MeV α + ^{154}Sm and 27 MeV ^3He+^{148}Sm have been measured. A front-back asymmetry is seen in the γ yield above the GDR region in both cases, providing model-independent evidence for a nonstatistical reaction mechanism. In addition, the measured high energy yields for E_γ>18 MeV are 2 to 3 orders of magnitude above calculations using the statistical model code CASCADE with ground-state GDR parameters.

These yields are suprisingly large for α's, where semidirect excitation of the giant dipole resonance should be small, since the α-target interaction is mostly isoscalar, and where direct dipole radiation is reduced by the effective charge factor $e^2_{eff}=\mu^2(Z_1/M_1-Z_2/M_2)^2$ (=zero for α + self-conjugate nuclei). To investigate this possible dependence on effective charge, we measured spectra at θ_γ=90° from 27 MeV α and ^3He bombarding ^{61}Ni, ^{95}Mo, ^{124}Sn, and ^{181}Ta. This selection of targets varied e^2_{eff} for α's from 0.024 to 0.14 and for ^3He's from 0.35 to 0.60. In all cases yields above statistical model calculations were apparent in the giant resonance region. Qualitatively, the nonstatistical yields from the α's strongly increase with target mass, and hence e^2_{eff}, while the nonstatistical yield from ^3He's is strong and greater than that from α's for all targets. The data are qualitatively consistent with a direct reaction mechanism for the α's; however, there is a suggestion of a split GDR strength function in the nonstatistical yields from α+^{154}Sm.[1] If this is true, it would require a nonstatistical reaction mechanism proceeding through the GDR, such as a semidirect process. The greater Q-value for the ^3He reactions (≈10 MeV greater than that for α's) makes it difficult to interpret directly the difference between the ^3He- and α-induced yields.

To compare more directly ^3He- and α-induced reactions, targets and bombarding energies were matched to form the same compound nucleus at the same excitation energy. The statistical γ yield of the reaction from these two different entrance channels is then essentially the same (calculations indicate that differences due to angular momentum are negligible) when scaled by the different fusion cross sections. Spectra for the formation of ^{65}Zn at E_x=29.3 MeV, ^{99}Ru at 28.2 MeV, and ^{123}Te at 28.5 MeV with ^3He and α entrance channels are shown in Fig. 3.5, along with statistical model calculations. In the formation of ^{65}Zn, the nonstatistical yield of the ^3He channel is greater than that from the α channel, while for the two heavier nuclei the nonstatistical yields from the two entrance channels are similar. It is difficult to understand the significance of these similarities on the basis of qualitative arguments, since the ^3He and α bombarding energies are substantially different in each case. For a more quantitative interpretation of these results, we are beginning to calculate the direct alpha reaction process.

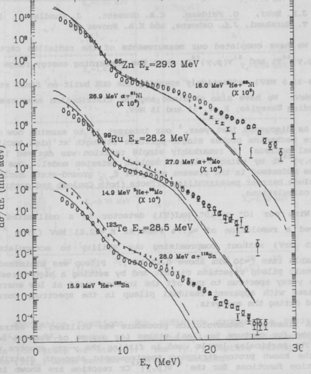

Fig. 3.5 γ-ray yields from the formation of the same compound nucleus at the same excitation energy with ^{3}He (circle) and α (X) projectiles. Solid (^{3}He) and dashed (α) lines are CASCADE statistical model calculations. Data are scaled for plotting purposes only.

Reference:

1. **Nuclear Physics Laboratory Annual Report, University of Washington (1984) p. 13.**

******

3.6 Excited-State GDR's in ^{46}Ti and ^{52}Cr via the (p,γ) Reaction

J.A. Behr, G. Feldman, C.A. Gossett, J. Gundlach, R.A. Loveman,*
T. Murakami, J.L. Osborne, and K.A. Snover

We have completed our measurements of the radiative capture reactions $^{45}Sc(p,\gamma)^{46}Ti$ and $^{51}V(p,\gamma)^{52}Cr$ over the bombarding energy range E_p=4–23.5 MeV (E_x=14–33.5 MeV), effectively spanning the GDR built on final states up to $E_x^f \leqslant 10$ MeV. We have also obtained angular distribution measurements at three bombarding energies, E_p=7, 11 and 15 MeV.

As discussed last year,[1] our interest is to examine how the (p,γ) GDR capture mechanism probes single-particle strength at high excitation in the residual nucleus. A remarkably simple relation was derived in the case of $^{27}Al(p,\gamma)^{28}Si$ by using a direct nucleon emission model.[2] One question that will be addressed in the present study of $f_{7/2}$ ground-state nuclei is the need to include barrier penetrability effects (both Coulomb and centrifugal) in the model calculations.

With our 10" × 10" NaI(Tl) detector in a collimated geometry, we achieved a resolution of ≈2.7% FWHM at E_γ=22.61 MeV (from $^{11}B(p,\gamma)^{12}C$ at E_p=7.25 MeV) without compromising our ability to accumulate data at a reasonable rate (≈50 kHz above 0.25 MeV). Pileup was minimized by using an electronic pileup rejection circuit and by setting a high threshold (≈8 MeV) in the γ-ray spectrum to cut off the intense yield at low energies. In the few cases with apparent residual pileup in the spectrum, corrections were applied during the analysis.

A lineshape deconvolution procedure was utilized to extract the (p,γ) strengths for capture to final states (or groups of states) below $E_x^f \approx 10$ MeV. The particular levels used in fitting the γ-ray spectra were selected from the known proton-stripping spectroscopic strength distributions. The excitation functions for the $^{51}V(p,\gamma)^{52}Cr$ reaction are shown in Fig. 3.6-1, where the (γ,p_0) cross sections were computed by detailed balance. Almost all of the plots indicate a broad resonance near $E_\gamma=E_{GDR} \approx 18$ MeV. The rather large width, particularly evident in the lowest three cases, possibly arises from isospin splitting of the GDR. This is not an uncommon feature in this mass region and, in fact, has been observed in photonuclear reactions on ^{52}Cr.[3] Similar effects have been reported in the case of the ^{46}Ti GDR as well.[4]

By comparing the excitation curves in Fig. 3.6-1 with the spectroscopic factors[5] plotted in Fig. 3.6-2, a qualitative sense of the correlation of the capture strength with $C^2S_p^+$ can be obtained. The GDR strength of the ground-state transition is weaker than that of the first excited state, and both are much weaker than the strength seen in the excitation function for the 3.11 MeV group of states; the $C^2S_p^+$ distribution shows the same trend. The excitation

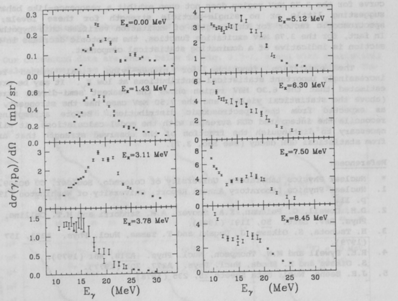

Fig. 3.6-1 Excitation functions for radiative capture to excited final states in $^{51}V(p,\gamma)^{52}Cr$. Plots are labelled by the excitation energy of the final state (or group of states). The (p,γ) capture strength has been converted to (γ,p_o) cross section by detailed balance.

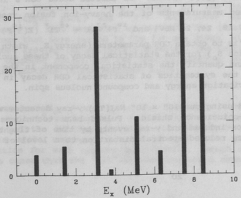

Fig. 3.6-2 Distribution of spectroscopic strength in ^{52}Cr obtained from the proton stripping reaction $^{51}V(^3He,d)^{52}Cr$.[5] Above E_x = 3 MeV the spectroscopic factors for individual levels have been summed in order to correspond to the groups of states for which excitation functions are plotted.

curve for the 3.78 MeV region does not even exhibit a resonance-like behavior, suggesting little or no single-particle strength for these levels; the spectroscopic factor for this region of excitation verifies this hypothesis. In fact, for the 3.78 MeV excitation function, the monotonic decrease in cross section is indicative of a dominating statistical component.

The excitation functions for higher-lying final states reveal increasingly important statistical contributions at low E_γ. It may be crudely estimated that the 6.30 MeV region shows the weakest semi-direct strength (above the statistical yield), and the 7.50 MeV case has the strongest, just as expected from the spectroscopic distribution. Before attempting to reconcile the integrated GDR strength with the model calculations, it will be necessary to distinguish the fraction of the observed strength that arises from statistical GDR decay (see Sec. 3.7).

References:

* Nuclear Physics Laboratory, University of Colorado, Boulder, CO 80309.
1. Nuclear Physics Laboratory Annual Report, University of Washington (1984) p. 11.
2. D.H. Dowell, G. Feldman, K.A. Snover, A.M. Sandorfi and M.T. Collins, Phys. Rev. Lett. 50, 1191 (1983).
3. H. Tsubota, S. Oikawa, J. Uegaki and T. Tamae, Nucl. Phys. A321, 157 (1979).
4. R.E. Pywell and M.N. Thompson, Nucl. Phys. A318, 461 (1979). S. Oikawa and K. Shoda, Nucl. Phys. A277, 301 (1977).
5. J.R. Beene, Nucl. Data Sheets 25, 235 (1978).

******

3.7 Statistical Decay of the Giant Dipole Resonance in ^{46}Ti and ^{52}Cr

J.A. Behr, G. Feldman, C.A. Gossett, J.H. Gundlach, J.L. Osborne, and K.A. Snover

In conjunction with our (p,γ) studies[1] of excited-state GDR's in ^{46}Ti and ^{52}Cr, we have performed measurements of the heavy-ion fusion reactions $\alpha + {}^{48}\mathrm{Ti} \rightarrow {}^{52}\mathrm{Cr}^*$ (E_α=12, 17.18, 24, 28 MeV) and $^{19}\mathrm{F}+^{27}\mathrm{Al} \rightarrow {}^{46}\mathrm{Ti}^*$ ($E(^{19}\mathrm{F})$ = 30, 40, 50, 60 MeV). Our goal is to obtain GDR parameters (energy E_0, width Γ and E1 sum rule strength fraction S_0) for the statistical decay of these nuclei in order to: 1) understand and quantify the statistical component in the (p,γ) reactions, and 2) examine the systematics of statistical GDR decay in these nuclei as a function of excitation energy and compound nucleus spin.

Spectra were measured using our 10" × 10" NaI(Tl) γ-ray detector with a plastic scintillator anti-coincidence shield. Pulsed beam techniques were employed to separate neutron-induced and γ-ray events by time of flight, and pileup rejection electronics reduced spectral distortion to a level of 7% or less. An additional subtraction of pileup events was done off-line to eliminate this effect.

Our corrected data are shown below in Fig. 3.7-1, along with statistical model calculations using the compound nuclear evaporation code CASCADE.[2] The

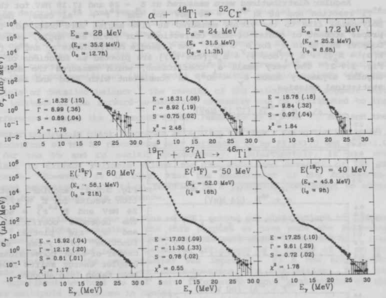

Fig. 3.7-1 Statistical γ-ray spectra for the heavy-ion fusion reactions $\alpha + {}^{48}Ti$ (upper plot) and ${}^{19}F + {}^{27}Al$ (lower plot). Solid curves are preliminary χ^2 fits generated by CASCADE. The final values of the three GDR parameters that were varied in the fit are given, with errors in parentheses. Also shown are the lab projectile energies, the initial excitation energies E_x of the compound nuclei and the critical angular momenta ℓ_0 for the initial spin distributions in the compound nuclei.

GDR parameters E_0, Γ and S_0 in the Lorentzian γ-ray strength function were varied in a χ^2 minimization routine to fit the region $E_\gamma > 12$ MeV. The results of the fitting procedure are displayed on the plots. With the analysis still underway, it may be too early yet to determine any GDR systematics for each nucleus specifically, though one may note in comparing the two cases that the ${}^{19}F + {}^{27}Al$ reaction has a consistently larger width and lower resonance energy than the α + ^{48}Ti case. In fact, this energy difference is in disagreement with the general $78A^{-1/3}$ MeV relation for GDR energy, which would predict a higher GDR energy in ^{48}Ti than in ^{52}Cr. The differences in the two reactions are still being investigated.

Angular distributions were measured at E_α = 24 and 17.18 MeV for the α + ^{48}Ti reaction and at E(^{19}F) = 60 MeV for the ^{19}F + ^{27}Al case. Legendre polynomial fits to the yields measured at five angles were computed, taking proper account of center-of-mass corrections for yield and angle, as well as Doppler shifts in E_γ for $\theta_\gamma \neq 90°$. The Legendre coefficients a_1 and a_2 [where $W(\theta) = A_0(1 + a_1P_1(\cos\theta) + a_2P_2(\cos\theta))$] are plotted as functions of E_γ in Fig. 3.7-2. The very small a_1 coefficient, which measures the degree of angular asymmetry about θ_γ = 90°, is consistent with zero and hence with statistical emission.

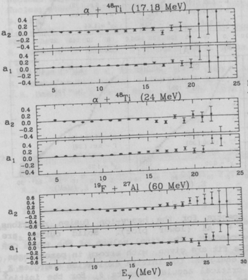

Fig. 3.7-2 Angular distribution results for E_α = 17.18 and 24 MeV and E(^{19}F) = 60 MeV. The Legendre coefficients a_1 and a_2 are plotted as a function of γ-ray energy. Center-of-mass conversions and Doppler energy shifts have all been taken into account.

References:

1. See Sec. 3.6 of this Report. Also, Nuclear Physics Laboratory Annual Report, University of Washington (1984) p. 11.
2. F. Puhlhofer, Nucl. Phys. A 280, 267 (1977).

******

3.8 Forward-to-backward Asymmetry in the (γ,n) Reaction in the Energy Range of 20-30 MeV

P.T. Debevec,* D.H. Dowell,† I. Halpern, L.J. Morford,* T. Murakami, D.W. Storm, and S.A. Wender+

As described in last year's Annual Report,[1] we studied the (γ,n) angular asymmetries in Pb and Cd at the University of Illinois in 1983. The forward-to-backward asymmetries were found to increase from small values (≃0.2) to large ones (≃0.6) around the energy where the isovector E2 giant resonance is expected to lie. In order to understand the observed behavior of the asymmetry curves we compared them with theoretical curves which we calculated using the direct-semidirect (DSD) model of capture reactions along with the principle of detailed balance.[2] The results of the calculations suggest that rapid increase of the forward-to-backward asymmetry can be attributed to the interference between the isovector dipole resonance at $E_x \simeq 78A^{-1/3}$ MeV and the isovector quadrupole giant resonance at $E_x \simeq 130A^{-1/3}$ MeV. Using the DSD model, the locations of the E2 resonances were estimated to be 23.5±1.0 and 26.5±1.0 MeV for the Pb and Cd nuclei, respectively. Unfortunately, it was not possible to extract reliable values for the width and strength of the E2 resonance. However, it is clear that the measurement of the forward-to-backward asymmetry in the (γ,n) reaction is a promising complement to other methods for studying this resonance.

In the forthcoming run in June we will extend our observations to lighter targets and higher energies. For this purpose we have made the following improvements. 1) Three new neutron detectors were made. Their use will lead to a multiplication of neutron detection efficiency by a factor of 6. 2) The neutron shield at the monochrometer was improved. 3) A new acquisition program was written to allow for event-by-event data acquisition. From the next experiment we hope to get more information about systematics of the higher multipole resonances in nuclei.

References:

* University of Illinois, Urbana, IL 61801.

† Brookhaven National Laboratory, Upton, NY 11973.

\+ Los Alamos National Laboratory, Los Alamos, NM 87545.

1. Nuclear Physics Laboratory Annual Report, University of Washington (1984) p. 16.
2. T. Murakami et al. (to be published).

4. HEAVY ION REACTIONS

4.1 Spin Distributions in Sub-Barrier Heavy Ion Fusion

D.D. Leach, T. Murakami, M.J. Murphy, A. Ray, C.C. Sahm, and R. Vandenbosch

There has been considerable interest in sub-barrier fusion cross sections following the observation of large sub-barrier enhancements which can depend on the nuclear structure of both the projectile and the target. The spin distribution of the compound nucleus is intimately connected to the energy dependence and the absolute magnitude of the sub-barrier fusion cross section. We have previously used a gamma ray technique to characterize the spin distribution.[1] We measured the gamma ray multiplicity for fusion events tagged by the detection of a discrete gamma ray in a particular evaporation channel. The broad spin distributions that we found at sub-barrier energies could be accounted for if we took into account both the penetrability of the centrifugal potential and the effects of target deformation. The disadvantage of this tagging method is that only even-even residual nuclei exhibit discrete gamma rays prominent enough to serve as a tag. Thus one can explore only those limited bombarding energy ranges where a particular suitable xn channel is dominant. At energies where the observed channel is not dominant, spin fractionation effects can distort the results, because predominantly low-spin compound states contribute near threshold and predominantly high-spin states contribute at bombarding energies where the (x+1)n channel is dominant.

We have begun a new experimental program to study sub-barrier spin distributions through fission fragment angular distributions. This is a particularly simple and unbiased method because for the nuclei being studied fission exhausts the total fusion cross section and there is no opportunity for spin fractionation. The mean square value of the spin distribution can be easily extracted from angular distributions if the distribution parameter K_o^2, given by the product of the effective moment of inertia and the nuclear temperature, is known. A fortuitous circumstance occurs for the compound nucleus ^{248}Cf. This nucleus has been formed by α-induced fusion with ^{244}Cm, and the K_o^2 value was determined from the easily specified spin distribution for above-barrier fusion with this light projectile. This same compound nucleus, ^{248}Cf, can also be formed by the reactions ^{12}C+^{236}U and ^{16}O+^{232}Th. We have measured the sub-barrier fission cross sections and fission angular distributions to probe the fusion probability and spin distributions for these two entrance channels.

An array of transmission-mounted solid state detectors whose thickness (~ 20 μ) is short compared to the range of the elastically scattered projectiles was mounted in the backward hemisphere. Absolute cross sections were determined by normalization to Rutherford scattering at more forward angles.

The fusion cross section excitation function for the ^{16}O+^{232}Th system is shown in Fig. 4.1a). Also shown are some measurements at higher energy by Back et al.[2] An angular distribution obtained at E_L=85.7 MeV is shown in Fig. 4.1b). The observed angular anisotropy is about twice what our preliminary calculations predicted for the case of full momentum transfer. Because the c.m. velocity, and thus the momentum transfer, influences the angular distribution, we made an additional coincidence measurement which confirmed that the fragments were indeed coming from a composite system with the beam momentum.

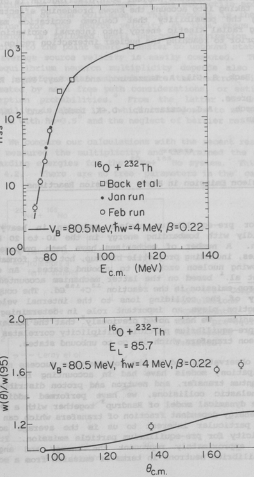

Fig. 4.1 a) Experimental fission cross sections (open and filled circles from present work, squares from Back et al.[2]) and fit with V_B=80.5 MeV, $\hbar\omega$=4 MeV, and β=0.22.
b) Experimental anisotropy (circles) together with expectations (full curve) based on fit to excitation function.

The fusion cross section was fitted using a model which takes into account both barrier penetration and target deformation effects.[3] This prescription has previously been successfully used to account for the spin distributions in the ^{12}C and $^{16}O+^{154}Sm$ systems. A preliminary fit to the fusion cross section is shown in Fig. 4.1a) and the anisotropy it predicts is shown in b). We do not understand the large discrepancy between the expected and observed anisotropies. The compound nuclear spin distribution is broader than expected even after taking into account the known broadening effects. We are presently exploring the possibility that Coulomb excitation may be preferentially converting radial kinetic energy into internal excitation for the lower partial waves prior to reaching the nuclear interaction region.

References:

1. R. Vandenbosch, B.B. Back, S. Gil, A. Lazzarini, and A. Ray, Phys. Rev. C 28, 1161 (1983).
2. B.B. Back et al., in press.
3. S. Gil, R. Vandenbosch, A.J. Lazzarini, D.-K. Lock, and A. Ray, Phys. Rev. C, in press.

******

4.2 Pre-Equilibrium Nucleon Emission in Heavy Ion Fusion Reactions

R. Vandenbosch

The probability for pre-equilibrium nucleon emission in heavy ion reactions increases rapidly with bombarding energy in the 10 to 20 MeV/A bombarding energy domain. A number of mechanisms have been proposed to account for these particles, including projectile breakup, hot spot formation, and nucleon escape following nucleon exchange to unbound states. An early calculation by Bondorf et al.[1] based on the latter mechanism accounted for many features of the neutron emission in the reaction $^{12}C+^{158}Gd$. The coupling of the relative velocity of the colliding ions to the internal velocity associated with Fermi motion plays an important role in determining the probability for this mechanism. We have noted previously[2] that the bombarding energy dependence of the pre-equilibrium particle multiplicity correlates well with the fraction of nucleon transfers which can go to unbound states.

Encouraged by this observation and by the considerable success nucleon exchange (one-body dissipation) models have had in accounting for energy dissipation, angular momentum transfer, and neutron and proton distributions in quasi and deeply inelastic collisions, we have performed additional calculations based on the dynamical model of Randrup[3] together with a phase-space calculation of the energy-dependent fraction of transfers which can lead to unbound states. Of particular interest to us is the average source velocity and the multiplicity for pre-equilibrium particle emission. It has been found possible to approximately represent the energy and angular dependence of the pre-equilibrium neutrons in terms of emission from a moving source which typically has a velocity intermediate between that of the projectile and the compound nucleus.

In the present calculations we divide the collision into a number of time intervals. The cumulative number of transferred particles during each interval is obtained from Randrup's dynamical transport model. This is multiplied by the fraction of such exchanges which lead to unbound states as determined by the displacement of the projectile and target Fermi spheres at this stage of the collision. This product is then used as the weighting function for the source velocity at this stage of the collision. The collision is followed until one-body dissipation has slowed the relative velocity to the point where transfer to unbound states is no longer possible. The average source velocity is easily computed. The absolute value of the pre-equilibrium neutron multiplicity depends also on the probability that after transfer to an unbound state the neutron will escape. This can be estimated by mean free path considerations, or estimated from optical model absorption probabilities.[4] From the latter we estimate that the escape probability is about 1/3, which corresponds to an average traversal distance of 4 fm with $\hbar\omega$=3.5[5] and the neglect of barrier reflection.

We compare our calculations with the recent results of Holub et al.[6] who have measured the multiplicity and determined the source velocity at three bombarding energies for the $^{20}Ne+^{165}Ho$ system. This comparison is shown in Fig. 4.2. There are no free parameters in the calculation of the average

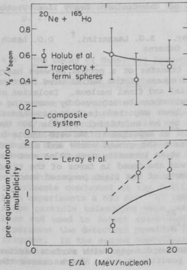

Fig. 4.2 Comparison of the present calculations (full curve) with experimental results of Holub et al. for pre-equilibrium neutrons in coincidence with fusion evaporation residues.

source velocity, and the calculated values compare well with experiment. The calculated multiplicities depend on our estimate of the escape probability, which may have an uncertainty of 25 or 30%.

It is interesting to compare the results of the present calculations with those which were reported recently by Leray et al.[6] The basic assumptions about the mechanism are very similar in the two calculations, although the detailed implementation of the transport model and of the neutron absorption are different. The two calculations appear to be in reasonable agreement.

References:

1. J.P. Bondorf, J.N. De, G. Fai, A.O.T. Karvinen, B. Jakobbson, and J. Randrup, Nucl. Phys. A 333, 285 (1980).
2. R.V. Vandenbosch, Nuclear Science Research Conference Series, Vol. 6, Harwood Academic Publishers, 1984.
3. J. Randrup, Nucl. Phys. A 327, 490 (1979).
4. BNL, 765.
5. A. Bohr and B. Mottelson, Nuclear Structure, Vol. I, p. 237 (1969).
6. E. Holub, D. Hilscher, G. Ingold, U. Jahnke, H. Orf, and H. Rossner, Phys. Rev. C 28, 252 (1983).
7. S. Leray, G. LaRana, C. Ngo, M. Barranca, M. Pi, and X. Vinas, Z. Phys. A 320, 383 (1985).

******

4.3 Progress Towards the Calibration of Sub-Coulomb Heavy Ion Proton Transfer Reactions

K.J. Davis, S. Gil,* M. Khandaker, A.G. Lazzarini,† D.D. Leach, R.A. Loveman,+ T. Murakami, and J.L. Osborne

The reaction cross section for the transfer of a proton between heavy ions involves the spectroscopic factor and square of the radial wave function of the transferred proton in both the initial and final nucleus. Isolation of these quantities for a particular configuration can be achieved by measuring a reaction triad. Two such schemes have been reported in previous Annual Reports.[1,2] The latter proposal proved to be unfruitful because of the difficulty of performing the ^{27}Al(^{42}Ca, ^{41}K)^{28}Si experiment. We were unable to resolve the first excited state of ^{28}Si from the ground state and also had difficulties maintaining a beam of ^{42}Ca 8^{+} at an intensity over 20 nA over the course of the experiment. This approach was abandoned in favor of the triad shown below which is actually a rearrangement of our first proposed reaction set.

a. ^{89}Y(^{15}N, ^{16}O)^{88}Sr

b. ^{89}Y(^{27}Al, ^{28}Si)^{88}Sr

c. ^{16}O(^{27}Al, ^{28}Si)^{15}N

Reactions a and b were measured at backward angles with surface barrier detectors. In each reaction there is a positive Q value which causes the ground state transfer peak to be higher in energy than the elastic peak. The sensitivity in this scheme is determined by the pile-up rate, whereas in the reversed reactions it is limited by the low energy tails of the elastic peaks. The elastic scattering cross section in the exit channels of these reactions was also measured to determine appropriate optical model parameters to be used in a DWBA calculation of the transfer cross section.

Four measurements were made in connection with reaction c. The momentum filter and Bragg curve spectrometer were used in conjunction to measure the ratio of the elastic and transfer reaction rates at 10 deg. in the lab. It was also necessary to measure the charge state distribution of the ^{16}O and ^{15}N ions. The absolute elastic cross sections in the entrance and exit channels were then measured with a gas delta-E E detector which detected recoil ^{27}Al and ^{28}Si ions at forward angles and permitted particle identification.

Analysis of these experiments is under way and it is anticipated that the extracted values of the product of the spectroscopic factors and squared radial wave functions will have an experimental uncertainty of 5% or less.

References:

* Comision Nacional de Energia Atomica, Buenos Aires, Argentina.
† Kaman Instrumentation, Colorado Springs, CO 80933.
+ University of Colorado, Boulder, CO 80309.
1. Nuclear Physics Laboratory Annual Report, University of Washington (1983) p. 27.
2. Nuclear Physics Laboratory Annual Report, University of Washington (1984) p. 27.

******

4.4 The Decay of Heavy-Ion Projectile Residues into Two Complex Fragments

D.D. Leach, M.J. Murphy, A. Ray, A.G. Seamster, and R. Vandenbosch

Heavy-ion projectile and target breakup reactions can produce multiple complex ($Z \geq 3$) fragments. We studied one of these reactions - the breakup of 20 MeV/n ^{35}Cl projectiles into two complex fragments - and obtained a detailed description of the sequence of events occurring during the reaction. The results show that both fragments come from the decay of an excited, long-lived precursor formed in an early stage of the reaction.

This conclusion was reached following two two-particle coincidence experiments conducted at the Holifield Heavy Ion Facility at Oak Ridge. In both experiments a 680 MeV ^{35}Cl beam bombarded a tantalum target. Four solid state particle telescopes were arrayed at small angles with respect to the beam and used to detect coincident projectile-like fragments. In the first experiment the detectors provided the charge and the total lab energy of each fragment. In the second experiment a position-sensitive detector element was added to each telescope to provide the relative kinetic energy of the two fragments as well.

We found that the ^{35}Cl projectile broke up into many different pairs of fragments of charge 3≤Z≤8. Our principle tool for determining the sequence of events leading to the production of these pairs was a Monte Carlo reaction simulation. This calculation could simulate simple two-step breakup reactions, in which the projectile collides with the target and loses some mass, travels out of range of the target's fields, and then breaks up into the observed fragments, and also the more complicated scenario in which the projectile-like product breaks up while still under the influence of the target's Coulomb field. We found that the simple, two-step calculation was fully consistent with correlations observed between the fragments' lab energies. This consistency disappeared when the target was brought close enough to the point of breakup to perturb the fragment energies. From this we deduced that the average excited ejectile travelled a considerable distance (≈ 300 fm), and thus lived a long time (5×10^{-20} seconds), before producing the observed fragments.

The lifetime of the projectile-like precursor is long enough for its excitation energy to equilibrate; one would thus expect it to be statistically distributed among the fragment excitation energies and relative kinetic energy in proportion to the density of excited states in each of the two fragments. Under this assumption one may calculate the analytic spectrum shape for the relative fragment energy for use as a fitting function. This function was found to completely describe the observed relative energy spectra, once it was corrected for the subsequent evaporation of nucleons from the excited fragments. (See Fig. 4.4 for a representative spectrum and fit.) Together

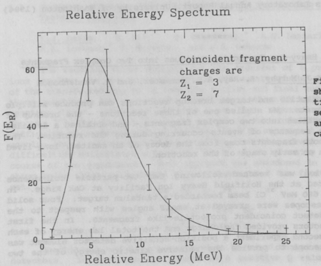

Fig. 4.4 The figure shows a representative spectrum of separation energy, and a two-parameter calculation.

with the inferred lifetime of the precursor, this shows that ^{35}Cl breakup into complex fragments is really a decay by an excited, long-lived projectile residue produced when the projectile collides with the target.

******

4.5 $^{28}Si+^{12}C$ Particle-γ Coincidence Measurement

D.D. Leach, K.T. Lesko, A. Ray, D. Shapira, and R. Vandenbosch

Recent backward-angle measurements of strongly damped reaction products from the $^{28}Si+^{12}C$,[1] $^{20}Ne+^{12}C$,[2] $^{16}O+^{27}Al$,[3] reactions have indicated the formation of a long-lived orbiting complex. Comparison of recent results[4] on the $^{24}Mg+^{16}O$ reaction with the $^{28}Si+^{12}C$ reaction demonstrates an entrance channel effect in these reactions and confirms that a non-compound process is dominant in these reactions.

We performed a particle-γ coincidence measurement to determine whether the ratio of the ^{12}C(g.s) to ^{12}C(4.44 MeV) yields is determined by phase-space considerations or enhanced by the structure of the orbiting complex. Compound nucleus model calculations predict that the multiplicity of the 4.44 MeV γ ray is about 0.5 at E_{Lab}=115 MeV and 145 MeV and the sticking limit prediction for the multiplicity of the 4.44 MeV γ ray is 1.00.

A ^{28}Si beam from ANL superconducting LINAC accelerator was used to bombard a natural carbon target. The beam was stopped by a tantalum foil, and a gas ΔE-solid-state E telescope was placed at 0° to detect carbon particles which were transmitted through the tantalum foil. About an inch-thick lead shroud with openings at both ends was placed around the tantalum foil to absorb low energy γ rays produced in the tantalum foil. An array of three 5" × 6" NaI detectors was placed in the backward hemisphere at 140°, 123° and 90°. The computer was triggered by coincidence and prescaled singles events. The γ-ray, TAC and particle spectra were recorded event by event. The efficiencies of the NaI detectors at 4.44 MeV were obtained by bombarding a carbon target with a proton beam and using known differential γ-ray cross sections, target thickness and total charge.

Fig. 4.5 shows the angular correlation of 4.44 MeV γ rays when a carbon particle is detected 0° telescope in the (-20.0 MeV≤Q≤-11.6 MeV) Q-value bin at E_{Lab}=143.6 MeV. The observed ($\sin^2\theta\cos^2\theta$) angular correlation in the c.m. frame implies that the ^{12}C is produced in an m=0 state. We observed the same angular distribution at all Q-value bins and bombarding energies. All magnetic substates can be populated in a compound nucleus decay. The observed enhancement of the m=0 state is consistent with the decay of the orbiting complex into an excited ^{12}C with its intrinsic spin colinear with that of the orbiting complex.

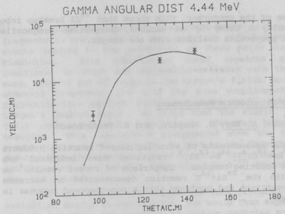

Fig. 4.5 The angular correlation of γ rays detected in coincidence with carbon particles in Q-value region (-20.0 MeV≤Q≤-11.6 MeV). The smooth curve shows ($\sin^2\theta\cos^2\theta$) dependence.

The carbon singles spectrum was dominated by random coincidences rather than the prescaled singles. The total number of angle-integrated 1.78 MeV γ-ray counts in the Q-value region(-6.5 MeV≤Q≤-2.0 MeV) was determined by assuming that the multiplicity of the 1.78 MeV γ ray is unity in that Q-value region. Then the total number of counts in the carbon singles spectrum in the Q-value region(-6.5 MeV≤Q≤-2.0 MeV) was normalized to that of the total angle-integrated 1.78 MeV γ-ray counts in the same Q-value region. The same normalization factor was used at other Q-value bins at the same bombarding energy. In this way, we obtained an upper limit for the multiplicity of the 4.44 MeV γ rays. We found that the average multiplicity of 4.44 MeV γ rays integrated over all Q values is less than 0.26 at E_{Lab}=145 MeV. This result is in disagreement with both the compound nucleus prediction (0.48) and the sticking limit prediction (1.00). We obtained similar results at E_{Lab}=115 MeV also. We are currently analyzing the ratio of protons to alphas in the coincidence data to obtain information about the average spin of the excited ^{28}Si.

References:

1. D. Shapira et al., Phys. Lett. B 114, 111 (1982).
2. D. Shapira, J.L.C. Ford Jr., and J. Gomez del Camp, Phys. Rev. C 26, 2470 (1982).
3. D. Shapira, J.L.C. Ford Jr., J. Gomez del Campo, and P.H. Stelson, Phys. Rev. C 21, 1824 (1980).
4. A. Ray et al., Phys. Rev. C 31, 1573 (1985).

******

4.6 Observation of Enhanced Transparency in Nucleus-Nucleus Total Reaction Cross Sections

J.G Cramer, A.J. Lazzarini,[*] D.D. Leach, R.A. Loveman,[†] W.G. Lynch,[+] T. Murakami, C.C. Sahm, M.B. Tsang,[+] D.R. Tieger, and J. Van der Plicht[+]

In a heavy ion collision at energies above about 20 MeV/A, the total reaction cross section is dominated by nucleon-nucleon effects and shows an energy dependence which reflects that of the n-n total cross section. Calculations[1] using a Glauber model which includes only such n-n effects have been found to agree remarkably well at bombarding energies above 20 MeV/A with available nucleon-nucleus data and with the rather small amount of nucleus-nucleus data, mainly on the $^{12}C+^{12}C$ system.

We have initiated an experimental program to obtain more data on nucleus-nucleus systems, particularly for systems heavier than $^{12}C+^{12}C$. We have measured total reaction cross sections with carbon ions at energies between 15 and 35 Mev/A using the K=500 superconducting cyclotron of the NSCL at Michigan State University. We have performed two measurement runs at the NSCL which took place in February, 1984 and March, 1985. In the 1984 run total reaction cross sections at laboratory bombarding energies of 15, 25, and 35 MeV/A were measured for the systems $^{12}C+^{12}C$ and $^{12}C+^{90}Zr$. The latter measurement provides for the first time a test of the energy dependence predicted by Glauber calculations for a heavier system. In contrast to observations with light systems, the decrease with energy in reaction cross sections for the $^{12}C+^{90}Zr$ system exceeds considerably that imposed upon Glauber calculations by the energy dependence of the nucleon-nucleon interaction.

The S-320 spectrometer of the NSCL was used to measure the forward angle elastic scattering. At each energy the elastic differential cross section data were fitted with several S-matrix models, and the S-matrix then used to determine the corresponding total reaction cross section. The overall total reaction cross section for each system at each energy was taken to be an average of these S-matrix fits. These experimental total reaction cross sections for two systems at three energies were compared with the predictions of the Glauber model.

The total reaction cross sections for the $^{12}C+^{12}C$ system were found to be in excellent agreement with both previous data for the same system and with Monte Carlo calculations of DiGiacomo and DeVries[2] and with simpler calculations of the authors using the Glauber model program of Peng.[1] This is shown in Fig. 4.6-1. The transparency, defined as the deviation of the measured σ_r from the Coulomb-corrected geometric cross section divided by the geometric cross section itself, was found to increase with energy as the Glauber model predicts.

In contrast, the measured σ_r values for the $^{12}C+^{90}Zr$ system, which are shown in Fig. 4.6-2, are in clear disagreement with Glauber model predictions made by the authors using the program of Peng.[1] Fig. 4.6-2 also shows a total reaction cross-section datum[3] measured using the transmission method for the $^{12}C+^{89}Y$ system and the Glauber model prediction for this system.

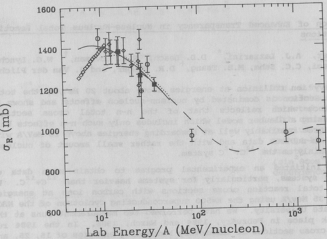

Fig. 4.6-1 Summary of total reaction cross section (σ_r) experimental data and calculations for the system $^{12}C+^{12}C$. The full curve is the prediction of a simple Glauber model calculation[1] performed by the authors. The dotted and dashed curves are the predictions of the more detailed microscopic Glauber model calculations of DiGiacomo and DeVries[2] using a deep and a shallow nuclear potential, respectively. The solid circles indicate present measurements, the open diamonds indicate other scattering measurements, the open squares indicate transmission measurements, and the single cross indicates a sum of directly measured reaction cross sections. Error bars for present work reflect both statistical and model-dependent systematic errors.

It is clear from Fig. 4.6-2 that the experimental total reaction cross-section data are significantly larger than the predictions at 15 MeV/A and significantly smaller than the prediction at 35 MeV/A. More significant is the energy dependence of σ_r, which is considerably stronger than the Glauber model predictions. This indicates a transparency which increases at twice the rate predicted by the Glauber model using the energy dependence of the free nucleon-nucleon cross section. Apparently the direct connection implied by the Glauber model between the energy dependences of the nucleon-nucleon total cross section and the total reaction cross section has failed for the latter heavy ion system.

The experiment run of March, 1985 was designed to expand the data set of total reaction cross sections for heavy systems and investigate further the unexpected energy dependence observed in the $^{12}C+^{90}Zr$ system. Elastic scattering data at 10, 15, 20, 25, 30, and 35 MeV/A were collected for the systems $^{12}C+^{40}Ca$, $^{12}C+^{90}Zr$ and $^{12}C+^{208}Pb$. These data are now being analysed.

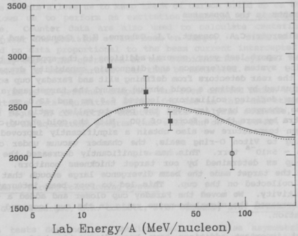

Fig. 4.6-2 Summary of total reaction cross section (σ_r) data and predictions for ^{12}C on mass 89 and 90 targets. The full curve is the the prediction of a simple Glauber model calculation[2] performed by the authors for the $^{12}C+^{90}Zr$ system. The dotted curve below it is a similar prediction for the $^{12}C+^{89}Y$ system. The solid squares indicate the results of the present work on $^{12}C+^{90}Zr$. The open circle shows a datum from a transmission measurement[3] for $^{12}C+^{89}Y$. Error bars for present work reflect both statistical and model-dependent systematic errors.

References:

* Present address: Kaman Instrumentation, Colorado Springs, CO 80933.
† Present address: University of Colorado, Boulder, CO 80309.
\+ National Superconducting Cyclotron Laboratory, Michigan State University, East Lansing, MI 48824.

1. R.M. DeVries and J.C. Peng, Phys. Rev. C 22, 1055 (1980); N.J. DiGiacomo, R.M. DeVries, and J.C. Peng, Phys. Rev. Lett. 45, 527 (1980).
2. N.J. DiGiacomo and R.M. DeVries, Comments Nucl. Part. Phys. 12, 111 (1984).
3. M. Buenerd, A. Lounis, J. Chauvin, D. Lebrun, P. Martin, G. Duhamel, J.C. Gondrand, and P. de Saintignon, Nucl. Phys. A 424, 313 (1984).

5. FUNDAMENTAL SYMMETRIES IN NUCLEI: $0^+ - 0^-$ ISOSCALAR PARITY MIXING IN ^{14}N

5.1 Improvements in the Apparatus

E.G. Adelberger, C.A. Gossett, J.L. Osborne, H.E. Swanson, and V.J. Zeps

Since our report last year, several additions to the apparatus have been made, improving system performance and diagnostic capability dramatically. Background in the rear detectors from defining slit and Faraday cup scattering has been eliminated by adding a cold shroud around the target and a pair of "clean-up" beam defining collimators located 6.8 mm and 12.0 mm from the target. These changes have improved the peak-to-valley ratio in the back detector spectra by more than a factor of 100. With the cold shroud cooled to liquid nitrogen temperature we also obtain a significantly improved vacuum. After upgrading to Viton O-ring seals, the chamber vacuum under operating conditions is ~ 5×10^{-8} torr. This has significantly decreased the rate of carbon build-up as determined by our target thickness monitors. Multiple scattering in the target made the beam divergence large enough that not all the beam was collected on the cup. This led to poor beam integration and feedback sensitivity. We moved the Faraday cup closer and added a +90 volt bias. This increased the signal-to-noise ratio in the cup loop and improved charge integration.

The most important additions have been diagnostic tools, namely an upstream steering magnet, a remote target positioning device and additional scalers. These have proven to be essential in understanding beam, target, and detector properties. The upstream steerer allows us deliberately to modulate the beam position in order to study false asymmetries. Results are discussed in Sec. 5.5. The remote target positioning device allows us to scan the target, making independent measurements at each target position. A more detailed discussion may be found in Sec. 5.3. We have added 24 scalers so that all signals from detectors, slits, and cup can be stored. We have also added a set of slits at the entrance to the beam line quadrupole to insure that the beam is centered through the quadrupole and to help diagnose possible aberrations in the focussing element.

We have steadily increased transmission from the low energy cup to the flap. We now routinely get ≈30% transmission at E_p=1.16 MeV and have seen a record 41% using an "unslacked" 3 μgm/cm^2 foil.

******

5.2 Improvements in the Data Acquisition Software

E.G. Adelberger, J.L. Osborne, R.J. Seymour, and H.E. Swanson

Features of the data aquisition program were described in last year's Annual Report. We have added some new on-line calculations as diagnostic aids in monitoring the experiment. Using data from the photomultipliers and the Faraday cup, the yield is calculated, which gives a measure of the target thickness. This allows us to keep track of carbon build up on the target. It also allows us to perform an excitation function to precisely locate the resonance. Counter data are also used to calculate centering asymmetries which monitor the position of the beam on target. A similiar calculation is performed on data proportional to the beam current intercepted by the slits and Faraday cup. The operation of the stabilization system, which keeps the beam centered in the apparatus, can thus be monitored.

An IBM PC-AT personal computer has been ordered which will become part of a portable data aquisition system for use in this and other experiments. Work has begun in converting existing data analysis software, which runs on our VAX, to an aquisition program that will run on the PC-AT.

******

5.3 Remote Target Positioning System

E.G. Adelberger, C.A. Gossett, J.L. Osborne, H.E. Swanson, and V.J.Zeps

In tests designed to obtain limits on false asymmetries from beam position modulation, we observed asymmetries which could be explained as target thickness variation effects. To study this, we designed and built a target positioning device. The main criteria in determining a final design were ridgidity, reproducibility, total scanning area and overall dimensions. The positioner, (shown in Fig. 5.3-1) consists of two precision lead screw

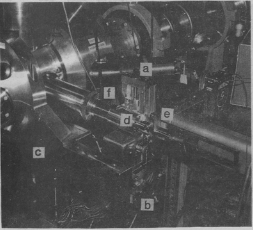

Fig. 5.3-1 The target positioning system. a) and b) Precision lead screw linear positioners.
c) Chamber support clamp.
d) Target ladder support.
e) Target ladder.
f) Welded bellows.

positioning tables (Velmex, Inc.) ridgedly mounted together at 90° for motion in both transverse (x,y) directions. The lead screws are driven by Slo-Syn stepping motors. The x,y-positioner is ridgidly clamped to the chamber, with the target ladder supported from the movable end. The target ladder support is mounted directly to the vertical positioner with the target ladder fed through to the chamber on sliding seals for changing targets. A welded bellows provides a flexible vacuum seal between the target ladder support and the chamber. The postioner allows us to scan across a 6.5 mm × 6.5 mm area of the target, making independent measurements at many locations.

A stepping motor controller was designed and constructed to operate the target positioners. It allows the target to be positioned manually from a local switch panel or remotely by the data aquisition computer. In the local mode of control, the speed may be varied over a large range for precise setting of the initial target position. To obtain sufficient torque from the motors, they are driven at about three times their rated current. The motors are protected from overheating by controlling their duty cycle and shutting off all current after rotation has stopped. In the remote mode of operation the computer varies the phases of the currents in each of the motor's windings with each new step. Thus, if there were a computer malfunction, the motor would just stop and power would be disconnected. This reduces the chance that a runaway motor might damage the target or bellows assembly. Code to run the stepping motors was written into the data aquisition program. The target is moved to a new position after each transfer of the scaler data to the computer and reset to its initial position after a complete data dump (Fig. 5.3-2).

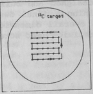

Fig. 5.3-2 Raster pattern used for changing target position. The dashed line indicates the return to the starting position. For a typical run, 100 - 200 separate measurements are made at each location.

The reproducibility of this system allows us to analyze our data as a function of target position. This has led to a much better understanding of target non-uniformity effects (See Sec. 5.5).

******

5.4 Fabrication of a Strip Target Polarization Analyzer

E.G. Adelberger, C.A. Gossett, and V.J. Zeps

We have chosen proton elastic scattering from ^{12}C near the 3/2+ resonance in ^{13}N at E_x=3.54 MeV (E_p=1.73 MeV) as a polarization analyzer for the parity mixing experiment. The reaction has large analyzing powers (see Sec. 2.2) at the angles of our counters, A ~ 0.9 for the back counters and ~ 0.6 for the front counters. We may take advantage of these large analyzing powers to measure small transverse polarization components in the longitudinally polarized beam. While the net transverse polarization of the proton beam may be zero, the spatial distribution of the polarization may not be uniformly zero. For example, a beam with circulating transverse polarization is one in which the outer edges of the beam have nonzero polarization; however, the up-down and left-right moments cancel to produce a net polarization of zero. The spatial distribution of transverse polarization components may be determined by sweeping a carbon strip target through the beam and measuring the left-right and up-down asymmetries as a function of position. The strip target should have a width smaller than the beam spot size, which is typically 1 mm × 3 mm.

A technique for producing carbon strip targets has been developed. Carbon foils 50 $\mu g/cm^2$ thick available commercially on glass slides are cut into slices approximately 2.5 mm wide. When floated from the slides the foils curl into tubes approximately 0.5 mm wide which are subsequently mounted on standard target holders. When used in conjunction with the remote target positioning system described in the preceding section, the targets may be used for measuring spatial uniformity of the proton beam polarization.

******

5.5 Limits on False Asymmetries Using Unpolarized Beam

E.G. Adelberger, C.A. Gossett, J.L. Osborne, H.E. Swanson, and V.J. Zeps

We have used an unpolarized beam to set limits on false asymmetries from several sources.[1] Limits on asymmetry from an unmodulated beam have been reduced to A_z(back-front)=$(1.3\pm3.6)\times10^{-6}$. This demonstrates that our data collection electronics have no substantial asymmetry. We have also studied false asymmetries that arise from beam position modulations. Modulation is done using a ferrite magnet similar to the beam stabilizing magnets.[2] Most tests have been performed with a position modulation of ±0.1 mm on target (the feedback stabilization reduces the actual modulation considerably). For comparison, a beam position modulation of $<5\times10^{-4}$ mm, with no stabilization, has been measured with the SIN[3] polarized source. Early measurements gave non-zero results as large as 10σ for A_z(back-front). These were eventually traced to a target non-uniformity effect. A difference in target thickness for the two beam positions leads to a non-zero value for A_z(front) and A_z(back). Because the cross-sections for the front and back counters have different energy dependences, exact cancellation does not occur when our signal A_z(back-front) is formed. A new target positioning system (see Sec. 5.3) allows us to measure and correct for target non-uniformities. Results from our first run with this system have demonstrated its utility. The data are shown in Fig. 5.5. Notice the large deviation in the count rate around position 9 due to a thick spot on the target. There is a

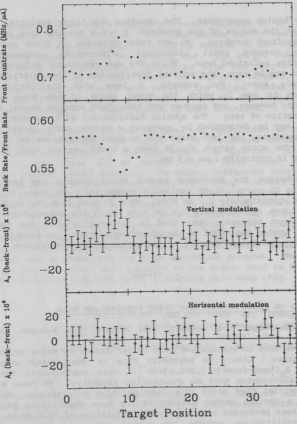

Fig. 5.5 A comparison of several measured quantities as a function of target position. The top panel shows the rate in the front counters. On the "bad" spot, the count rate increases by 10% and the ratio back rate/front rate, shown in the second panel, has a marked change as well. The bottom two panels show A_z(back-front) measurements for vertical and horizontal modulation.

correspondingly large change in the ratio back rate/front rate. Because of this ratio change, position modulation can produce a false asymmetry. The large asymmetry from the vertical modulation on the "bad" spot confirms this effect. For the horizontal modulation there is no apparent affect. This is due to the shape of the beam spot (1 mm high × 3 mm wide). The 3 mm wide beam spot "washes out" the effect for horizontal modulation. The results for vertical modulation, including the "bad" spot, are A_z(back-front)=$(3.3\pm1.2)\times10^{-5}$. When the "bad" spot is excluded, A_z(back-front)=$(1.5\pm1.3)\times10^{-5}$. For horizontal modulation, results are A_z(back-front)=$(-0.4\pm1.2)\times10^{-5}$, with little change of this value when the "bad" region is excluded. These results are very encouraging, because they allow us to exclude results in an unbiased way. At any rate, when these asymmetries are scaled to the expected position modulation of an atomic beam ion source, they are negligible compared with the expected PNC asymmetry of $\approx3\times10^{-5}$.

References:

1. Nuclear Physics Laboratory Annual Report, University of Washington (1984) p. 45.
2. Nuclear Physics Laboratory Annual Report, University of Washington (1984) p. 40.
3. R. Balzer et al., Phys. Rev. C, 30, 1409 1984.

6. FUNDAMENTAL SYMMETRIES IN ATOMS: PARITY MIXING IN HYDROGEN AND DEUTERIUM

6.1 Installation and Alignment of the New H-Atom Solenoid

T.A. Trainor and P. Wong

After characterizing a set of 20 aluminum pancake coils for a new solenoid,[1,2,3] we assembled them into an operating solenoid on a temporary support jig. A computer program was used to estimate the currents required through the various pancakes. A shunt system and shims were used to tune the B-field produced to a uniformity of two parts in 10^4 (of the total field magnitude) in both axial and transverse directions over a region ≈25" in length. The field uniformity achieved was limited by noise produced by the field measurement system.

Bolstered by this success we removed the old copper solenoid[4] from the H-atom apparatus so we could assemble the new aluminum one in its place. At this time we measured the fields produced by the old solenoid and found variations in the transverse direction of 3 parts per 1000.

We then installed the aluminum pancakes on the stainless steel liner and attached the shunt board and current control system. Before tuning the solenoid to an ultimate uniformity of a few parts in 10^5 we decided to increase the sensitivity of our B-field measurement system, and to investigate and remove any systematic errors introduced into the B-field scans. Electrical noise in the Hall effect system of the order of a few parts in 10^4 was traced to capacitive coupling from the solenoid/power supplies to the unshielded Hall probe cable. This was eliminated by grounding the solenoid and track system. The rabbit and track system were modified to reduce the mechanical jitter produced in the Hall probe when scanning the B-field.

The net result of these improvements is to make scans reproducible to ≈1 part in 10^5. However, a single scan does not discriminate between variations in the B-field itself and apparent variations caused by probe angle and position changes due to track irregularities. In order to utilize the improved signal-to-noise ratio of B-field scanning system we must separate track-induced variations from actual variations in the field. This has been accomplished by rotating the track 180° about the solenoid axis and subtracting the two scans obtained (see Figs. 6.1-1 and 6.1-2). Most track-dependent variations cancel except for two:

1) The position and angles of the track axis are different after the rotation. This requires that the track be re-centered. The resulting error is proportional to dB_z/dz and is negligible to a part in 10^5 over the region of interest, where the rf cavities are located.

2) The track exhibits a small but observable sag due to gravity (from 0.7 to 5 parts in 10^4 depending on track orientation) which does not flip as the track is rotated 180°. This effect must be compensated before scans with an accuracy better than 1 in 10^4 can be made. By loading the track with lead

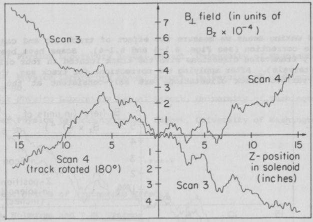

Fig. 6.1-1 Two scans of the transverse B-field showing the presence of a net transverse field variation. Scan 4 is taken with the track rotated 180° from the position used for scan 3. Both of these scans are rotated 90° from the scans in Fig. 6.1-3.

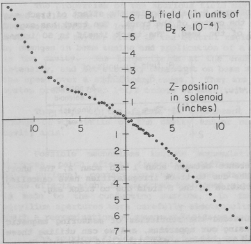

Fig. 6.1-2 A plot of the difference between scan 3 and scan 4. The track irregularities have cancelled out, again leaving only a smooth variation in the B-field due to misalignments in the positioning of the individual pancakes. In this orientation, the effect of track sag is ≈7 times less than the effect shown in Figs. 6.1-3 and 6.1-4. Therefore, no correction for track sag was made.

blocks and making scans we measure the effect of track sag and can apply an appropriate correction (see Figs. 6.1-3 and 6.1-4). Scans have been made in the x and y transverse directions with the track rotated in four orientations (at 90° intervals). After applying the corrections for track sag, the results from the various track orientations are self-consistent at the level of 3×10^{-5}.

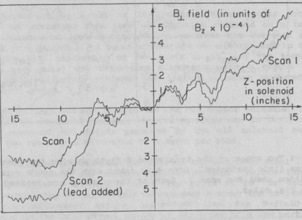

Fig. 6.1-3 Two scans of the transverse B-field showing the effect of track sag due to adding 2.0 Kg of lead to the center of the track. The track has sagged ≈0.004 inches under the weight of the lead. The track itself is 50 inches long.

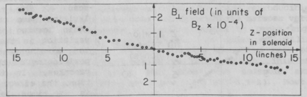

Fig. 6.1-4 A plot of the difference between scan 1 and scan 2. The short wavelength variations in the scans due to track irregularities have cancelled out, leaving only the smooth variation in the B-field due to track sag.

We feel that we now understand the subtleties of measuring magnetic fields down to ≈1 part in 10^5 using our apparatus, and we can utilize these measurements to tune our solenoid to produce a magnetic field with this degree of uniformity.

References:

1. Nuclear Physics Laboratory Annual Report, University of Washington, (1981) p. 28.
2. Nuclear Physics Laboratory Annual Report, University of Washington, (1984) pp. 48-50.
3. Nuclear Physics Laboratory Annual Report, University of Washington, (1984) p. 50.
4. Nuclear Physics Laboratory Annual Report, University of Washington, (1979) pp. 28-30.

******

6.2 Current Status of Systematic Effects

D.W. Holmgren and T.A. Trainor

Previously we have observed spurious axial electric fields which peak 1-2 cm inside the ends of each RF cavity with peak values of ~ 1 V/cm. Various diagnostic techniques allow precise determination of these field magnitudes and shapes via interferometric techniques using the metasable beam. These spurious fields form a serious limitation to the PNC measurement, and so we have expended some considerable effort to characterize them carefully and attempt strategies of elimination.

The properties of the spurious field may be summarized as follows. The large fields near the ends of the cavities remain constant in time and have been reproducible as long as these measurement techniques were available. The small (~ 20 mV/cm) field in the central region of the cavity can be changed by changes in beam tuning and application of a small (<2 mV/cm) axial AC field in the cavity. The large fields at the ends are also independent of beam intensity, and not strongly dependent on beam speed. (It is difficult to vary the speed over a significant range.) They are also not strongly dependent on system pressure over 1-1/2 orders of magnitude.

The sign of the fields is consistent with accumulation of positive change on the walls of the cavity and/or negative space charge along the cavity axis.

Possible mechanisms include accumulation of charges on insulating surfaces, patch effects (potential differences among crystal zones on the metal surface), contact potentials, and adsorption of hydrogen gas. All of these effects might be expected to change significantly if a dramatic change is made to the conducting surface. In fact, the copper cavities with beryllium apertures were carefully electropolished and gold plated, following which a reexamination of spurious fields was made.

The spurious fields (except for the small (~ 10 mV/cm) variable central component) were unchanged in all respects, we conclude from this result that surface effects on electrodes are not the primary source of the spurious field.

An alternative source of fields may be space charge production by the fast (500 eV), intense neutral hydrogen beam. This may occur either by collisions with background gas or by collisions with aperture edges. Comparing the ion production rates for gas collisions and aperture collisions we find that apertures dominate by about four orders of magnitude.

Production of charge on apertures is an attractive model because we know that the field shape, peaking near the cavity ends, is independent of cavity length. The model has difficulties in detail, because we observe that the field strength is independent of beam intensity. To retain the model we must come up with some saturation effect which determines the scale.

This spurious field presently limits the sensitivity of the PNC measurement to a level C_{2p} ~ 100 which is more than 1000 times the predicted value in the Standard Model. Refinements in the magnetic field described in the preceding section should reduce the sensitivity to this spurious field by 10-100 times. Strategies for directly reducing the spurious field should produce a reduction of more than 10 times.

7. MEDIUM ENERGY PHYSICS

7.1 A Model for Inclusive Scattering and Reaction Cross-Sections for Pions

K.G.R. Doss, I. Halpern, M. Khandaker, D.W. Storm, and D.R. Tieger

The nuclear reaction cross section for a projectile depends on the projectile's chance to have an interaction in the nucleus in which it loses some energy. For incident pions this cross section can be related to the inclusive scattering inelastic cross section if one assumes that (1) all pion interactions in a nucleus initially involve a single nucleon and that (2) inelastically scattered pions only rarely have more than one collision in the nucleus before they escape. A simple model was constructed which is based on these assumptions (for which there is abundant evidence below the (3,3) resonance) and on the additional assumption that the π-N interaction in the nucleus is the same as it is for free particles.

The model was studied to see how well it accounts for the considerable amount of data on pion reactions that is now available. In using the model to estimate cross sections it was necessary to include a number of fairly obvious effects (e.g., those of the Coulomb field on the geometry of the trajectories and on the pion kinetic energies). For positive pions with energies up to 100 MeV the resulting predictions of reaction cross sections and inclusive differential cross sections at 180° were then found to be in reasonable agreement with a large amount of data. For example, the estimates based on the model reproduce, fairly well, the observed magnitudes of the cross sections as well as their dependences on incident energy and on target mass. They also fit the observed ratios of charge exchange to normal scattering cross sections for both π^+ and π^-.

In view of these successes, it is particularly significant that the model considerably overestimates ratios of observed π^- to π^+ cross sections. For example, in heavy nuclei the expected reaction cross-section ratios are typically around 1.7 (largely due to Coulomb effects) whereas the cross-section ratios deduced from data (spallation studies; fission cross-sections; adding absorption to scattering cross sections) are only about 1.3 on the average. The predicted π^-/π^+ ratios for 180° scattering are even larger than those for the reaction cross sections, but the observed ratios are close to 1.2. It is not clear how much of these discrepancies arises from misinterpretations of the data or from a fundamental failure of the model. The details of the model and the comparison of its predictions with our data and with those of others have been recently submitted for publication.[1]

Reference:

1. K. Aniol, D.T. Chiang, K.G.R. Doss, I. Halpern, M. Khandaker, D.W. Storm, D.R. Tieger, P.D. Barnes, B. Bassalleck, N.J. Colella, S.A. Dytman, R.A. Eisenstein, R. Grace, C. Maher, D. Marlow, P. Pile, R. Rieder, F. Takeutchi, and W.R. Wharton, submitted to Phys. Rev. C.

******

7.2 Inclusive Scattering of Pions from Very Light Nuclei at 100 MeV

J.F. Amann,[*] W. J. Burger,[†] K.G.R. Doss,[+] D.H. Dowell,[×] I. Halpern, M. Khandaker, D.D. Leach, T. Murakami, D.W. Storm, and D.R. Tieger.

In continuing our systematic study of inclusive inelastic pion-nucleus scattering below the (3,3) resonance energy region, we measured in 1984 inclusive energy spectra of 100 MeV positive and negative pions scattered from ^{2}H, ^{3}He, ^{4}He, and ^{14}N. One motivation for studying the inclusive scattering of pions from these targets is to learn about the interplay of quasi-elastic scattering and pion absorption in the very simplest nuclei where effects due to multiple scattering and final-state interactions are expected to be minimal.

The experiment (Exp. 224) was performed at TRIUMF on the M11 channel. A QQD spectrometer, in conjunction with a high pressure (100 atmosphere) gas target, was used for measuring the momentum spectrum of the scattered pions. Some details of the experiment have been reported earlier.[1] We have essentially finished the analysis of our data. The shapes of the scattered pion energy spectra for all four targets are roughly as expected from a quasi-elastic scattering picture. The absolute cross-sections for ^{2}H, ^{3}He and ^{4}He (obtained from normalization to our hydrogen data and the known $\pi^{\pm}$-proton cross sections) compare well with earlier measurements at similar energies. The π^{+} inelastic scattering angular distributions for ^{2}H, ^{3}He, and ^{4}He in the back hemisphere (θ_{lab} ≥75°) are very similar to the free π^{+}-proton angular distribution at 100 MeV. In Fig. 7.2 we show the inelastic angular distributions together with a curve for the free π^{+}-proton distribution. The ^{14}N distribution is seen to be somewhat steeper with angle than the free π^{+}-proton distribution in accord with our earlier findings[2] in the mass region A=12-208.

The experiment was designed to compare the pion yields from ^{2}H, ^{3}He and ^{4}He directly. In comparing the ratios of inelastic π^{+} yields from ^{3}He and ^{4}He we find that ^{3}He yield is always higher than that of ^{4}He throughout our measured angular range. For π^{-} scattering, however, the corresponding inelastic yield is always lower. The cross-section ratios can be qualitatively understood by considering the number of nucleon types in these two nuclei, the large energy gap in ^{4}He reflecting the absence of excited states below the particle breakup energy, and the role of the extra neutron in ^{4}He in pion absorption.

In order to understand our findings quantitatively we have begun by carrying out a PWIA calculation using realistic wave functions for π^{+} scattering from ^{2}H. The results of our calculations are in reasonable agreement with our data and those of others within the assumptions of the impulse approximation. We are in the process of doing similar calculations for π^{+} scattering from ^{3}He and ^{4}He. Effects due to pion absorption have not yet been included in any of our calculations.

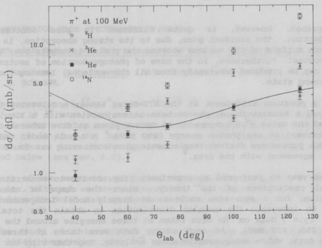

Fig. 7.2 Angular distribution of 100 MeV π^+ inelastic scattering on ^{2}H, ^{3}He, ^{4}He, and ^{14}N. The curve is the free π^+-proton angular distribution.

References:

* Los Alamos National Laboratory (LAMPF), Los Alamos, NM.
† Massachusetts Institute of Technology, Cambridge, MA.
\+ Lawrence Berkeley Laboratory, Berkeley, CA.
× Brookhaven National Laboratory, Upton, NY.
1. Nuclear Physics Laboratory Annual Report, University of Washington (1984) p. 52.
2. K.Aniol et al., submitted to Phys. Rev. C.

******

7.3 Coherent π^0 Photoproduction in the Δ(1232) Region

E.J. Beise,* E.C. Booth,† W.J. Burger,* G.W. Dodson,* D. Fleming,† S. Gilad,* J.P. Miller,† R.P. Redwine,* B.L. Roberts,† and D.R. Tieger

The close relationship in nuclei between pion-induced reactions and pion photoproduction in the energy region of the Δ(1232) resonance has long been recognized. Once the Δ is formed, its propagation in the nuclear medium and its subsequent decay is considered to be the same in either case. The nuclear volume probed, however, is quite different in pion scattering and photoproduction. The incident pion, due to its strong absorption, is confined to the back surface of the nucleus whereas the photon interacts over the whole nuclear volume. Furthermore, in the case of photoproduction of neutral pions, the pion can be produced coherently from all the nucleons, leaving the nucleus in the ground state.

In a previous experiment at the MIT-Bates Linear Accelerator (Exp. 82-04) we used a bremsstrahlung photon beam in conjunction with a liquid helium target and the Bates π^0 spectrometer to detect pions at five laboratory angles (25-80 degrees) at one photon energy (290 MeV).[1] A Δ-hole model calculation using input parameters derived from elastic pion scattering was found to be in excellent agreement with the data.[2]

Last year we performed an experiment (Exp. 83-19) to constrain further the model predictions of the theory. Since the shape of the angular distribution, for a spin-zero nucleus, is largely model independent, it is possible to integrate the angular distribution to obtain the total cross section. (γ,π^0) data on ^{4}He were taken at three energies around the Δ region (E_γ=210, 250, 330 MeV). At each energy data were taken at three angles. These new data, which are presently under analysis, together with our previous result at 290 MeV will exhibit the energy dependence of this reaction. Comparison of the peak position and energy width, as well as the magnitude, of the total π^0 photoproduction cross section with the predictions of the theory should provide a sensitive test of the Δ-hole model.

References:

* Massachusetts Institute of Technology, Cambridge, MA 02139.

† Boston University, Boston, MA 02215.

1. D.R. Tieger, E.C. Booth, J.P. Miller, B.L. Roberts, J. Comuzzi, G.W. Dodson, S. Gilad, and R.P. Redwine, Phys. Rev. Lett. 53, 755, (1984).
2. J.H. Koch and E.J. Moniz, Phys. Rev. C 27, 751 (1983).

8. ACCELERATOR MASS SPECTROMETRY (AMS)

8.1 AMS with Carbon and Beryllium: C-14 and Be-10 Radiochronology*

D. Balsley, G.W. Farwell, P.M. Grootes,† G.M. Hinn, D.D. Leach, and F.H. Schmidt

Measurements of $^{10}Be/^{9}Be$ and $^{14}C/^{12,13}C$ isotopic fractions in the range of 10^{-11} to 10^{-14} have been continued, and we are now able to measure the ^{14}C content of modern carbon samples from environmental materials with accuracy in the range of 1% to 1.5%, based upon two or more measurements each lasting about one hour. Some of the improvements that have made this possible are discussed below (see Sec. 8.2).

Most of our measurements during the reporting period have been made on ^{14}C samples, although we have measured the ^{10}Be content of a few surface snow samples from the South Pole in preparation for more extensive ^{10}Be work on ice cores.

The study of thin-sections of Sitka spruce annual tree rings (1962 through 1964), begun last year,[1,2] has been completed. The rapid changes in atmospheric $^{14}CO_2$ concentration caused by the nuclear weapons testing of 1962 and early 1963 are clearly reflected in the tree-ring cellulose. The growing season generally lasts from early May through September with most of the tree-ring growth (at a rate of 10% per week) occurring from mid-May to mid-July. The ^{14}C concentrations of equal growth increments (ten per year) plotted on this growth time scale compared well with published ^{14}C concentrations in atmospheric CO_2, and we conclude that the tree-ring cellulose responds very rapidly -- within days, or a very few weeks -- to changes in the atmospheric $^{14}CO_2$ concentration.

In another study involving very small (1-5 mg) carbon samples, undertaken with colleagues in the School of Oceanography, we have measured the ^{14}C concentration in two fractions of dissolved and of particulate organic carbon isolated from water samples of the Amazon River collected under the auspices of the CAMREX project. The acid-soluble fulvic acid fraction of the dissolved carbon showed a significantly higher ^{14}C concentration than the alkali-soluble humic acid fraction. Both contain a large fraction of post-1962 "bomb carbon." The coarse particulate fraction has the current atmospheric ^{14}C concentration, while the fine (smaller than 63 μm) particulates are significantly lower in ^{14}C and must include some pre-1950 organic material. Understanding the sources of organic material transported by the Amazon River to the ocean is essential for constructing the carbon cycle in the Amazon basin; since the Amazon is a very large contributor to the fresh-water-borne organic carbon content of the ocean, this will also be important to the understanding of the global CO_2 budget.

Further study of our background confirms the findings in this laboratory and elsewhere that even for accelerators long used for nuclear physics experiments the contribution of the AMS system itself to a measured ^{14}C background is typically very low. In our case it is <0.06% of modern carbon, corresponding to an apparent age of about 60,000 years. This low machine background will be advantageous in the measurement of "very old" samples (materials whose age is greater than, say, 40,000 years); such measurements will be undertaken in the year immediately ahead.

References:

* Our work has been supported in part by the M.J. Murdock Charitable Trust and the National Science Foundation (Grant EAR-8115994, Environmental Geoscience Program).

† Quaternary Isotope Laboratory, University of Washington.

1. Nuclear Physics Laboratory Annual Report, University of Washington (1984) p. 54.
2. G.W. Farwell, P.M. Grootes, D.D. Leach, and F.H. Schmidt, Nucl. Instrum. Methods B5, 144 (1984).

******

8.2 AMS: Technical Improvements

D. Balsley, G.W. Farwell, H. Fauska, P.M. Grootes,* D.D. Leach, and F.H. Schmidt

Our continued efforts toward more accurate normalization of ion beams (e.g., ^{14}C against ^{13}C or ^{12}C) have been fruitful and, as mentioned above, we now measure $^{14}C/^{13}C$ with an accuracy of 1% to 1.5% for modern carbon. A central feature of the present apparatus is a system that provides rapid, nuclear-magnetic-resonance-controlled shifting of the magnetic elements in order to change quickly from one isotope to another.[1] Data-taking is now also greatly facilitated by a recently-accomplished integration of the TI-Controller-operated sample-alternation sequence, the NRM-controlled isotope-alternation system, and the PDP-11/60-controlled data-collection routine; the new system reduces the elapsed time for a measurement cycle and requires far less human intervention.

Important recent technical advances include also the successful reduction of CO_2 from natural materials to elemental C for the preparation of AMS samples (graphitized pellets). A hydrogen reduction process, catalyzed by iron powder, is used and can now be carried out routinely.

Improvement of overall ion transmission was accomplished, and the AMS measurements were rendered less sensitive to small fluctuations in accelerator parameters, by realignment of a beam line and the associated magnetic quadrupole.

A new modification to the sputter ion source is under development, and this project will be given high priority during the next few months.

References:

* Quaternary Isotope Laboratory, University of Washington.
1. Nuclear Physics Laboratory Annual Report, University of Washington (1984) pp. 55,56.

9. RESEARCH BY OUTSIDE USERS

9.1 Measurement of Total Body Calcium by Neutron Activation

C.H. Chesnut,* B.L. Lewellen,* and R. Murano*

We have now completed 16 years using neutron activation to measure total body calcium in patients with bone wasting disease.[1] In the past year we performed 153 patient irradiations. Two therapeutic regimes were under test. Under the first regime, patients were treated with 1.25 dihydroxy calciferol (vitamin D).[2] Under the second regime, patients were treated with a sequential dosage of phosphate and didronel[3] and were followed after withdrawal of the drug. In both studies, an equal number of untreated control subjects were followed and many other tests were performed as well as neutron activation. Since June, 1982 we have also been measuring the bone mineral in the lumbar spine by the dual photon absorbtion technique developed by Mazess of the University of Wisconsin and applied extensively by Wahner and Riggs of the Mayo Clinic.

References:

* Division of Nuclear Medicine, University of Washington.
1. Nuclear Physics Laboratory Annual Reports, University of Washington (1967-1982).
2. Hoffman-LaRoche Laboratories.
3. Proctor and Gamble.

******

9.2 Irradiation of Optical Materials

K.L. Ballou,* B. Bohnhoff-Hlavacek,* T. Criswell,* and A.R. Tokuda*

Track structure mechanisms in optical materials are being studied using a wide range of ion species and energies. Results of this study are being applied to the fabrication of anti-reflective coatings using the track-etch process.

Reference:

* Boeing Aerospace Company, Seattle, WA 98124-2499

******

9.3 Light-Ion Irradiation Creep

E.R. Bradley,* C.H. Henager, Jr.,* and E.P. Simonen*

The U.S. Department of Energy, Office of Basic Energy Sciences, supports a Radiation Effects on Metals and Ceramics Program at Battelle, Pacific Northwest Laboratory (PNL). A light-ion irradiation creep experiment, as part of the PNL research program, is being conducted at the Nuclear Physics Laboratory at the University of Washington. Ferritic steel specimens were bombarded with 15 MeV deuterons from the Van de Graaff accelerator to observe *in situ* radiation hardening in ferritic alloys.

Two ferritic alloys, Fe - 1.1 Ni - 0.05 C and Fe - 1.1 Ni - 0.3 Cu - 0.03 C, at a temperature 673 K with an applied stress of either 35 or 45 MPa were bombarded with 15 MeV deuterons. Irradiations were continuous for 24 hours at a damage rate of 6×10^{-7} dpa/s, resulting in a total dose of 0.05 dpa. The tests were performed in a manner consistent with previous PNL creep experiments on pure nickel.[1] Preliminary results indicate that ferritic steels undergo both irradiation creep enhancement and radiation hardening in much the same manner as fcc metals. The steel containing 0.3% copper appeared to harden more than the steel without copper, as expected. Models of radiation hardening will be constructed from the strain rate data as a function of fluence.

References:

* Pacific Northwest Laboratory, Richland, WA 99352.

1. C.H. Henager, Jr., Ph.D. Dissertation, University of Washington (1983).

10. ACCELERATORS AND ION SOURCES

10.1 Van de Graaff Accelerator Operations and Development

J.F. Amsbaugh, J.R. Cromie, H. Fauska, D.J. Hodgkins, C.E. Linder, F.H. Schmidt, R.E. Stowell, T.D. Van Wechel, W.G. Weitkamp, and D.I. Will

The major effort at the tandem during the year centered around preparation for installation of the superconducting booster, which is described in Sec. 13 of this report. In order to make room for the new ion source injector deck, the injector tandem will have to be removed. Consequently, the injector tandem is being dismantled. Since this machine was of a unique design and had a somewhat checkered career, a brief history of it is given in Sec. 10.5.

The Accelerator Mass Spectrometry (AMS) group must use the signal from the generating voltmeter (GVM) to regulate the tandem terminal voltage since the beam current used in their experiments is too small to produce a slit signal in the conventional way. Oxide layers on the surface of the GVM vanes can inject noise into this signal. Gold plating the GVM vanes has reduced beam position fluctuations by about a factor of two when regulating the terminal voltage with the GVM.

Insertion of a grid into the aperture of the first active electrode of the low energy beam tube of the tandem improves the transmission of heavy ion beams. Transmission is sufficiently improved to make its use essential for AMS. However, the grid injects electrons into the beam tube which lead to tube breakdowns and degrades the performance of the machine. Magnetic suppressors at the grid surface are partially effective in reducing the effects of these electrons. Increasing the field at the grid surface from about 350 G to 500 G by replacing alnico suppression magnets with cobalt-rare earth magnets increases the useful terminal potential.

The HVE inclined field beam tubes used in our machine normally have small magnets attached to the first 20 electrodes to supress electrons. (These first electrodes are flat, not inclined.) The field produced by the magnets is so small, less than 50 G, that it should have negligible effect. As an experiment, we tried removing the magnets. The high voltage performance of the machine with the grid deteriorated, but performance without the grid was unaffected. In fact, the machine ran very well at a terminal voltage of 9.6 MV for more than a week without the magnets.

Further accelerator modifications required by the AMS group are described in Sec. 8.1.

The charging belt was replaced May 8, 1984. The replaced belt was one of the best we have had; it ran 10,800 hours before failing. Other maintenance on the tandem was routine.

During the year from April 16, 1984 to April 15, 1985 the tandem operated 5236 hours. Additional statistics of accelerator operations are given in Table 10.1.

Table 10.1
Tandem Accelerator Operations
April 16, 1984 to April 15, 1985

Activity		Days Scheduled	Percent
A. Nuclear Physics Research			
Light Ions		101	28
Heavy Ions		103	28
Radiochronology		53	15
	Total	257	71
B. Outside Users			
Battelle Northwest Laboratories		9	2
The Boeing Company		5	1
	Total	14	3
C. Other Operations			
Accelerator Development		22	6
Accelerator Maintenance		34	9
Unscheduled Time		38	11
	Total	94	26
	Grand Total	365	100

******

10.2 Cyclotron Operations and Development

J.R. Cromie, H. Fauska, B.L. Lewellen,* R. Murano,* R.E. Stowell, and W.G. Weitkamp

The 60 in. cyclotron, which first operated at "a satisfactory operational level" in November 1952, continues to run, although on a considerably attenuated schedule. The maintenance problems encountered during the year resulted mostly from aging parts and components. The vacuum system presented the most difficulties; many of the rubber gaskets installed in the 1940's have succumbed to radiation or chemical damage and begun leaking. The automatic frequency control was completely rebuilt to take advantage of modern circuitry to eliminate a number of chronic problems. This is described in Sec. 10.6.

The cyclotron is now used almost exclusively for the *in vivo* calcium measurements conducted by the Division of Nuclear Medicine, described in Sec. 9.1.

The machine ran 143 hours between April 16, 1984 and April 15, 1985. It was scheduled for 72 days. Approximately 10 days were lost to operations because of maintenance problems.

Reference:

* Nuclear Medicine, University of Washington.

******

10.3 Predicting Tandem Parameters

W.G. Weitkamp

New accelerators are nearly always built so that beam-optics parameters such as lens and steerer settings can be set automatically by a computer. Retrofitting all the power supplies of an older machine so that a computer can set parameters automatically is probably not cost effective. Never-the-less, there are many cases in which the operator of a tandem accelerator can use the guidance a computer can supply, especially if the operator is inexperienced with the beam being accelerated.

We have completed a program TANDEM to assist in setting up our accelerator. The program asks for the required ion species energy and for information about the configuration of the machine. It then calculates all beam-optics power supply settings and predicts the beam transmission, using simple algorithms or interpolating between sets of parameters known to give a good accelerator tune. The information is printed out in a form similar to an accelerator log sheet.

The program calculates charge state fractions using standard formulas[1] and predicts maximum expected source output on the basis of past experience or, in the case of unusual ions from the sputter source, from tables describing experience elsewhere.[2] TANDEM works well for the common beams from the active ion sources. Using the program can reduce the time required to set up a beam from several hours of knob twiddleing to a few minutes.

References:

1. V.S. Nikolaev and I.S. Dimetriev, Phys. Lett. 28A, 277 (1968).
2. R. Middleton, Nucl. Instrum. Methods 144, 373 (1977).

******

10.4 Crossed-Beams Polarized Ion Source

D. Badt, J.G. Douglas, A. Herron, J.R. Olson, J.L. Osborne, T.A. Trainor, and V.J. Zeps

We have conducted high voltage tests of the cesium gun electrodes and operated the various cesium heater elements for long time periods to check for design flaws and spark damage. These tests have gone well, after installation of additional transient suppression in a few critical areas. Most recently we have extracted a cesium beam of several milliamperes. Higher beam intensities are temporarily prevented because cooling lines for beam tubes and the calorimeter are not completed. However, this intensity at first operation is very satisfying.

There is a short list of remaining assembly items for the source. Some high-voltage wiring and a cooled baffle for the cesium neutralizer cell need to be installed in the neutralizer spool. Support stands for the second 90° electrostatic inflector and spin precessor need to be manufactured. The vacuum box, support standard and some final machining need to be done for the last two 90° inflectors. And the atomic beam source rf system and spin-flip telemetry need to be installed. We expect to operate cesium gun and AB source together within a month and produce a negative hydrogen beam.

The production of this source is a continuing saga. At this time last year we undertook a contract with GMW Inc., instigated by them, to provide certain design and construction services for the project. The contract represented about half of the remaining design and construction, with the other half, plus all integration work, to be done by NPL personnel. The GMW designs were consistently late, and by September, the end of the contract period, no construction had been started. The contract was terminated with a token payment for the partial design package. This cost the project about six months.

In order to minimize the impact of this delay some of the GMW contract funds were used to hire machining time at three campus machine shops, and an additional machinist was hired at NPL. By this means we have reduced the impact of the GMW default by about two months.

******

10.5 The Tandem Injector

W.G. Weitkamp and staff

The injector tandem was decomissioned on December 1, 1984 to make room for components of the superconducting booster. Some of the high (or low) points in the history of this machine are listed below. For more detail see Ref. 1.

When the accelerator was installed, the injector tandem was in the "neutral-negative" configuration shown in Fig. 10.5.a. A duoplasmatron ion source with a hydrogen gas charge-exchange canal located outside the injector pressure vessel produced a neutral beam, typically equivalent to about 1 mA at 45 keV. This beam drifted to the terminal of the HVEC model FN voltage generator, which was run with negative potential. At the terminal, charge exchange in hydrogen gas produced a beam of negative ions. 5 large mercury diffusion pumps and a pumping tube in the pressure vessel provided pumping for the charge-exchange canals.

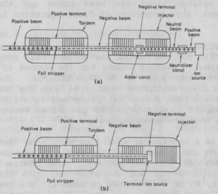

10.5 Accelerator configurations: a. neutral-negative, b. terminal source.

The injector was ordered as part of the accelerator system in 1961. The factory ran into problems meeting negative beam specifications and delayed shipping until 1966. The truck carrying the injector pressure vessel from the factory hit a low bridge, knocking the vessel off the truck. After returning to the factory for repair and recertification, the tank was loaded on a railcar. The car was derailed in Ohio. Fortunately, this time the tank was not damaged, so it arrived in Seattle somewhat battered, but ready for installation. The installed injector was accepted in the fall of 1967.

The injector was immediately put to use. Early experiments using protons and deuterons from the injector included measurements of proton-proton bremstrahlung, (d,p) and (p,t) reactions on light and medium weight nuclei to study reaction mechanisms and energy levels, analog resonances in Pb using elastic and inelastic proton scattering, giant resonances using (p,γ) reactions, and spin flip probability in (p,p'γ) reactions. During its first full year of operation, the injector was used 46% of the time.

The injector produced up to 1.2 μA of negative hydrogen ions at a maximum terminal voltage of 7 MV and about 20 nA of negative oxygen ions. The transmission of the hydrogen ions through the tandem was almost 100%. It was pointed out[2] that when the injector was operating at 7 MV and the tandem at 9 MV, giving 25 MeV protons, the accelerator was producing the highest energy direct current beam of protons available in the world at that time. It held that record until the Brookhaven double MP tandem accelerator came on line in 1969.

On September 20, 1969, a glass-to-metal seal in the beam tube in the terminal of the machine cracked, admitting high pressure tank gas to the vacuum system of the machine. The resulting shock wave displaced the beam tubes axially about an inch, knocked over a large 16 in. diffusion pump, but otherwise did little damage, primarily because several vent valves had been installed on the vacuum system outside the pressure vessel, in anticipation of such an accident.

In 1971, it was decided to install a direct extraction ion source in the terminal of the injector, converting to the configuration shown in Fig. 10.5.b. This source[3] was completed in 1974 and produced up to 10 μA of hydrogen ions, several μA of oxygen ions and 1 μA of chlorine ions. It was much simpler and easier to operate than the neutral source, but was difficult to maintain because of its inaccessibility inside the pressure vessel.

The injector operated a total 17,900 hours. During the first years of its existence, it was an invaluable tool and helped put the Laboratory at the forefront of many important fields of nuclear research. However, shifting Laboratory research priorities and the tight operating budgets of the 1970's reduced demand for the injector so that by 1980 it was not always kept in operating condition. Negotiations are presently under way that should lead to a reincarnation of this machine as a stand-alone tandem in another laboratory. We wish it sucess.

References:

1. W.G. Weitkamp and F.H. Schmidt, Nucl. Instrum. Methods 122, 65 (1974).
2. H.E. Wegner, Bull. Am. Phys. Soc. 14, 204 (1969).
3. Nuclear Physics Laboratory Annual Report, University of Washington (1974) p. 11.

******

10.6 Cyclotron Frequency and Grid Drive Controller

H. Fauska

The controller which holds the cyclotron oscillator frequency constant and which provides proper oscillator grid drive has been redesigned, constructed and installed.

The original control was prone to instability and poor regulation. Following a tank spark the controls did not return to the operating point corresponding to the same ion orbital current peak as that just prior to the spark. We therefore chose to redesign the circuit utilizing more modern components.

Fig. 10.6 is a block diagram of the new circuit. The 11.47 MHz cyclotron RF and the RF from a 10.59 MHz crystal oscillator are mixed in a balanced mixer to provide a difference signal of 0.88 MHz. The difference frequency is then mixed in a second balanced mixer with the output of a variable RF oscillator. The second mixer output is 0-80 kHz. The output of the second mixer is shaped and buffered to supply signals to a console frequency meter and the frequency high/low difference amplifiers. The difference amplifiers drive the respective correction relays.

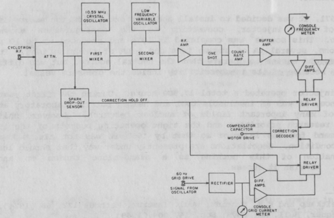

Fig. 10.6 Block diagram of the automatic frequency/grid drive controller.

Because frequency correction of the tank compensating capacitors changes the oscillator grid drive and vice versa, the automatic frequency and the grid drive correction relays must be decoded and gated to minimize hunting. The decoder then drives the correct motor to change the tank compensating capacitor.

The grid drive correction is sensed from a 60 Hz signal developed at the oscillator housing. The 60 Hz signal amplitude contains information about the grid drive. After rectifying, the grid drive signal is supplied to a console meter and to difference amplifiers. The difference amplifiers drive relay drivers producing grid high or grid low error correction signals. The correction signals are then supplied to the compensator motor drive decoder.

The spark dropout sensor monitors the cyclotron oscillator output. If the RF remains correct, power is supplied to operate the two sets of correction relays. In the event of a tank spark the relay power is cut off and all corrective action is inhibited for a pre-set hold-off time.

The newly designed circuit returns the cyclotron to the original ion orbit current peak, but the thermal change of tank components during sparking causes some damped hunting action upon return. The overall operation and maintenance requirements are greatly improved.

11. NUCLEAR INSTRUMENTATION

11.1 Design and Construction of Electronic Equipment

H. Fauska, J.M. LaCroix, D.B. Newell, R.E. Stowell, T.D. Van Wechel, and M.R. Walker

A majority of the electronics shop time this past year was devoted to projects on the booster linac, described in Sec. 13 of this Annual Report. The following major projects were carried out and are described in detail in the indicated sections.

a. A prototype linac resonator controller was designed and built for use in the linac satellite control stations (see Sec. 13.6).

b. Modifications and design changes were made to a Stony Brook resonator controller board for use in our version of a resonator controller (see Sec. 13.9).

c. Electronics for pretandem beam buncher was designed and constructed (see Sec. 13.15).

Other booster linac projects include the following:

a. A constant current source temperature box was built for monitoring various cryogenic temperatures in the linac test cryostat.

b. A cavity simulator was constructed to allow testing of the linac control electronics.

c. A fast divide by 3 ECL circuit was built to divide down the 150 MHz master clock from the linac for use in the buncher.

Several additional electronic projects were undertaken.

a. A prototype laboratory universal regulated power supply card with variable voltage and current limits was designed and constructed.

b. A circuit was designed to allow the ND2400 multichannel analyzers to dump their data into the VAX computer. Two back plane cards for the ND2400's were built.

c. Two NIM module universal logic boxes were designed and constructed.

d. Several temperature controller modules were built for the new polarized ion source.

e. Once again, the number of computer terminal outlets in the laboratory was expanded, for a total of 32.

f. Additional high quality 50 ohm cabling was run between the caves and counting rooms.

******

11.2 Measurement of the Lineshape Efficiency of the 25.4 cm × 25.4 cm NaI Spectrometer

E.G. Adelberger, K.A. Snover, P.B. Fernandez, C.A. Gossett, J.L. Osborne, and V.J. Zeps

We have measured the photopeak efficiency of our NaI spectrometer for $E_\gamma \approx 2$–15 MeV. We used the reactions $^{12}C(^3He,p\gamma)$ and $^{13}C(^3He,p\gamma)$ and detected γ rays in coincidence with protons populating the 2.313 MeV and 4.915 MeV levels in ^{14}N and the 8.313 MeV level in ^{15}N. These states have large branching ratios to the ground state and decay isotropically in the CM (all have $J \leq 1/2$); the p-γ angular correlation is therefore known.

The γ-ray coincidence spectra were fitted using the following lineshape:

$$Y(E) = A_2 \times \left\{ \frac{\exp\left[-\frac{[E-E_\gamma']^2}{2\sigma^2}\right] + R_1 \exp\left[-\frac{[E-[E_\gamma'-0.511]]^2}{2\sigma^2}\right]}{\sqrt{2\pi\sigma^2}} + \frac{R_2 \,\mathrm{erf}(E) \times \left[a_o + a_1 \exp\left[\frac{E-E_\gamma}{a_2}\right]\right]}{a_o E'_\gamma + a_1 a_2 [1-\exp[-E_\gamma'/a_2]]} \right\},$$

where $E_\gamma' = E_\gamma + A_1$,

$a_1 = 1 - a_o$,

$$\mathrm{erf}(E) = \int_E^\infty \frac{\exp\left[-\frac{[E'-E_\gamma']^2}{2\sigma^2}\right]}{\sqrt{2\pi\sigma^2}}\, dE'$$

The lineshape constants σ, R_1, R_2, a_o, and a_2 were determined as a function of E_γ by fitting spectra with isolated γ rays. When the detection efficiency was measured, only the energy shift A_1 and the strength A_2 were varied in order to minimize χ^2. Our code then calculated the fitted area of the photopeak (defined by $0.7\,E_\gamma \leq E \leq 1.1\,E_\gamma$). The NaI photopeak efficiency is then

$$\eta(E) = \frac{\text{photopeak fitted area}}{\text{proton yield}} \times \frac{1}{\text{branching ratio}} \times \text{dead time corrections}$$

$$\times \text{ CM to laboratory frame transformation}$$

We measured $\eta(2.313\ \mathrm{MeV}) = (1.754\pm0.043)\times10^{-3}$

$\eta(4.915\ \mathrm{MeV}) = (1.786\pm0.062)\times10^{-3}$

$\eta(8.313\ \mathrm{MeV}) = (1.874\pm0.068)\times10^{-3}$

To determine the efficiency at 15.065 MeV, we measured the resonance yield for the $^{12}C(p,\gamma_o)$ reaction ($E_p \approx 14.25$ MeV). We used a thick (170 mg/cm^2) natural carbon target and detected γ rays at $\theta_{lab}=125^o$. Under these conditions the size of the step in the thick target yield is known to be $(6.83\pm0.22)\times10^{-9}\gamma_o$'s per incident proton.[1] We measured $\eta(15.065\ \mathrm{MeV}) = (1.684\pm0.064)\times10^{-3}$. Our results are shown in Fig. 11.2.

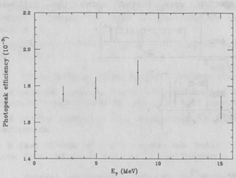

Fig 11.2 Measured efficiency for the 25.4 cm × 25.4 cm NaI spectrometer.

Reference:

1. R.E. Marrs, E.G. Adelberger and K.A. Snover, Phys. Rev. C 16, 61 (1977).

******

11.3 RAYTRACE Calculation for the Momentum Filter

K.J. Davis and T. Murakami

As we reported in the last year's Annual Report,[1] the focal plane of the momentum filter turned out to be nearly 20 cm down-stream of its designed position. In order to understand this rather disappointing feature, we decided to re-calculate ray trajectories in the momentum filter using the program RAYTRACE.[2] Since this program has been successfully used for designing sophisticated spectrometers all over the world, main efforts were concentrated on getting reliable field parameters for the actual magnets. All parametrizations were made based upon the field maps supplied by the manufacturer (ANAC). Dipole field calibrations used in the calculations were ones obtained last year following a standard procedure, namely the currents were set to 400 A and then slowly stepped down to the desired setting. Quadrupole calibrations were based on our new measurements but the absolute values were normalized to the ones provided by the manufacturer. Therefore the quadrupole setting might still have some uncertainty.

The newly obtained parameters for the magnets were somewhat different from those used for final adjustments in the magnet alignment.[3] Especially rotation angles for both entrance and exit edges of uniform and non-uniform field dipole magnets were considerably smaller than those used for the previous calculation. The fringe fields for quadrupole and uniform field dipole magnets were fairly well reproduced by new parameters, but there is an appreciable difference between actual and parameterized fields for the non-uniform field dipole magnet.

The predicted momentum dispersion at the focal plane agreed reasonably well with the measured one in the momentum range of -11.5% to +15%. The position of the focal plane was predicted 8.4 cm down-stream from the physical center of the momentum filter. This value was still not enough to account for our observation, i.e. about 20 cm down-stream. In order to obtain better agreement we had to increase the strength of the quadrupole magnet by 12.5% in the calculation. The predicted value changed to 16.8 cm down-stream by using this strength. Clearly we have to measure an absolute strength of the quadrupole to get a more definite answer.

Further investigations are now in progress to determine possible ways of improving the momentum filter performance.

References:

1. Nuclear Physics Laboratory Annual Report, University of Washington (1984) p. 79.
2. J.E. Spencer and H.A. Enge, Nucl. Instrum. Methods 49, 181 (1967).
3. Nuclear Physics Laboratory Annual Report, University of Washington (1982) p. 155.

*****

11.4 Target Preparation

G.M. Hinn

In Table 11.4 are listed a few of the more interesting of the 180 targets prepared in the Laboratory last year.

Table 11.4

Target	Starting Form	Final Form	Method of Preparation	Backing	mg/cm^2 Thickness
$^{9,10}BeO$	Ice, Alaska South Pole and carrier ^{9}Be	$^{9,10}Be$	chelex ion exchange	none	1,5
$Ti^{15}N$	Ti metal	$Ti^{15}N$	^{15}N nitriding high temperature	S.S.	1,2,3
Al_2O_3	Al metal	oxide	anodization	S.S.	0.2
^{40}Ca	carbonate	metal	reduction-evaporation	S.S.	1
^{58}Ni	metal	metal	resistive heating	S.S.	0.1,0.3
$^{nat,28}Si$	oxide	metal	reduction F-bombardment	S.S.	1,2,3
^{15}N	melamine	melamine	resistive heating	Ta	0.2,0.3
^{64}Zn	oxide	metal	electrolytic reduction and evaporation	Pt	1
^{nat}Sm	oxide	metal	H_2 reduction	Ta	2
$^{nat,89}Y$	metal	metal	vacuum evaporation	20 µg C, 150 µg Al	0.05
^{208}Pb	oxide	metal	H_2 reduction	S.S.	1
^{nat}Th	metal	metal	vacuum evap.	Ni	0.3,0.4

a. Cracked slacked ethylene stripper foils. We have been routinely making 3 $\mu g/cm^2$ cracked slacked carbon stripper foils. Most heavy ion experimenters prefer thinner foils because of greater transmission. However, it has been found that 3 $\mu g/cm^2$ unslacked cracked ethylene foils give approximately 30% more transmission than do 3 $\mu g/cm^2$ slacked cracked ethylene foils. The lifetime is shorter for the unslacked foils but for some experimenters, including the Accelerator Mass Spectrometry (AMS) group, transmission is more important and heavy foil damage does not occur. Therefore, we are loading 15% of our foil wheel with 3 $\mu g/cm^2$ unslacked cracked ethylene foils.

b. ^{40}Ca. An experiment at Michigan State University required the production of 1 mg/cm^2 oxygen and carbon free ^{40}Ca metal targets with the dimensions 2.5 cm × 2.5 cm. This required making the targets at M.S.U. two weeks before the experiment using their facilities. This worked well as they have modernized their target lab and have converted their diffusion pumped vacuum bell jar system to a cryopumped system. This provides an environment for the production of targets free from carbon, which is always present in a system pumped by an oil diffusion pump. They also have built a high vacuum target storage system as well as a vacuum transfer system all of which provide the necessary equipment for fabricating self supporting ^{40}Ca targets free from low Z containments.

12. COMPUTER SYSTEMS

12.1 Data Acquisition System Enhancements

H.P. Readdy, R.J. Seymour, and E.G. Tieger

Our principal data acquisition system consists of a DEC PDP 11/60 computer with two 5 megabyte RL-01 disks, a 1600 bpi 75 ips 9 track tape drive, a Printronix P-300 printer/plotter with a Trilog Tektronix hardcopy board, a DEC VT-11 graphics display, a Tektronix 4006 terminal and a BiRa MBD-11 controlling a CAMAC crate to connect with twelve Tracor Northern TN-1213 ADCs. Fifteen 75 MHz scalers are read via an IEEE-488 bus interface. The CAMAC crate contains an additional 48 scalers in LeCroy 2551 modules, as well as a LeCroy 2249A 12 Channel ADC, two LeCroy 2228A TDCs and a LeCroy 2256A Waveform Digitizer.

New Data Acquisition Hardware

The DEC 11/60 received an RL-02 disk drive, doubling its total disk space to 20 megabytes.

LeCroy loaned us a 2249W 12-channel ADC for testing with longer-duration gates than a 2249A can reliably sustain. The consequences of testing that unit are discussed in Sec. 12.3 of this report.

The VAX is now actively involved in data collection by controlling the Lab's ND2400 multichannel analyzers. The original scheme was breadboarded with a cheap commercial microcomputer and then transferred to a simple circuit card mounted in each ND2400. The ND2400s can be plugged into any terminal port in the building and can be controlled from any other. The spectra are transferred to Lab-standard SINGLES format disk files.

New Data Acquisition Software

The MBD-11 was programmed to provide a continuous readout of all 48 LeCroy 2551 scalers during a SINGLES data collection run. The code handles 24-bit overflows to provide an effective 40 bits of precision (a little over 10^{12}). The 11/60's VT-11 program was modified to provide an optional continuous display of the 48 values.

The radiochronology group now uses the 11/60's ability to read and control the currents through the quadrupoles, steering magnets and momentum filter to flip between different isotopes of carbon during their runs.

The MBD-11 has been programmed to control an X/Y stepper motor system for the ^{14}N parity experiment. This code uses the 11/60's UNIBUS and Q-BUS to allow one "intelligent peripheral" (the MBD-11) to control another 11/60 peripheral (a DRV11).

The ^{28}Si + ^{12}C particle gamma coincidence experiment group tested our 2228A TDCs in an attempt to replicate a "shoulder" seen in their data from

Argonne. The code developed for that was also used to test the 2249W. As mentioned above, those runs are detailed in Sec. 12.3

******

12.2 Data Analysis System Enhancements

D.A. Patterson, H.P. Readdy, R.J. Seymour, and E.G. Tieger

Our data analysis system consists of a 4 megabyte DEC VAX 11/780 with dual RK-07 disks, two Systems Industries disks totalling 1 gigabyte, three 9 track and one 7 track tape drives, a Printronix P-300 printer/plotter, a Hewlett Packard 7475A pen plotter, an AED-512 color graphics display, two dial-in lines and about thirty local terminals of varied lineage.

Hardware Developments

Once more, the major acquisition for the data analysis system was more disk capacity, this time in the form of a Fujitsu 600 megabyte non-removable drive. It shares the SI 9900 controller with the 414 megabyte Eagle drive added last year. It has been logically "split" into two 300 "drives". One will serve as the system disk when we install VMS version 4, while the other has entered service as a "scratch" disk. People using the computer may create temporary files of a size limited only by the free space on the disk. Since the VAX uses disk space to effect its "virtual memory" scheme, this new scratch space allows programs (such as CASCADE and the shell model code) freedom to carry their analysis much further than before.

The advent of accurate, inexpensive pen plotters has caused the overdue retirement of our 1965 CalComp plotter. It was replaced by an HP 7475A. Plots it had generated were presented at a conference one week after unpacking it. The quality of the plots is reflected by the drawings throughout this annual report.

The VAX has been brought to its simple-to-attain memory limit of 4 megabytes. Any further expansion will require the replacement of the entire memory system or the addition of a second memory system. Either way, the next step will be very expensive.

We have begun adding DEC VT-220 emulating terminals to our system. We are using them as VT-100 emulators now, but DEC's VMS V4 and future products will make use of the expanded keyboards and display functions.

Software Developments

In support of the new HP plotter, any program which used the Calcomp was either modified or replaced.

The SLAC package TOPDRAWER and its prerequisite Unified Graphics System was imported from Argonne and installed. It was modified to match our hardware mix and expanded to include the HP plotter. It quickly took over the bulk of the Lab's standard data plotting duties.

Oxford's FIGURE (in our DRAW) was also modified to drive the HP plotter.

We have installed a software driver for the AED-512's DMA board. This allows the entire screen to be written or read back in under 1 second. So far the only application program which uses this is one which draws a Tektronix image on the screen, and then reads back the "rasterized" image for direct printing by the Printronix. This process is much faster for complicated plots than the normal Printronix rasterizing software.

The public-domain program HOST provides simple control and support for the modems. It was imported from the UW Physics VAX and modified for our modem's protocols. We also have XMODEM, another public-domain program which allows error-checked transfers of files between our VAX and most CP/M microcomputers.

As expected, the VAX has figured as the principal development machine and simulation engine for modelling the LINAC's operation. This has consumed days of cpu time during such tasks as calculating the beam optics.

The VAX also serves as the editing and compilation machine for the LSI-11 based satellite controllers for the resonator RF, cryogenics and vacuum systems. Programs developed in MicroPower Pascal are "downloaded" to the satellite computer via one of the VAX's terminal lines.

The SINGLES analysis program HP has received its usual round of minor improvements, primarily correcting bugs and improving the user interface. It received display reformatting options to match DRAW plots. It was modified to allow negative counts in data channels.

******

12.3 A Gating Problem in LeCroy CAMAC Modules

C.A. Gossett, R.J. Seymour, K.A. Snover, R.E. Stowell, and T.D. Van Wechel

For many years we have seen an occasional problem when running a LeCroy 2249 12-channel charge sensitive ADC in "SINGLES" mode. It occurred irregularly, and usually with high (greater than 20 kHz) event rates. The module simply "locks up". This is caused by a linear gate arriving during the module's internal CLEAR cycle. The gate causes the gate lock-out circuits to trigger, but CLEAR prevents the actual start of a conversion. Thus an end-of-conversion never occurs, and that in turn prevents the eventual generation of a CAMAC LAM or Q. The result is a module with a locked ADC, no conversion, and no CAMAC signals announcing the fact.

Attempts to block the gates by raising the CAMAC crate's INHIBIT signal were fruitless, since LeCroy has INHIBIT block the *trailing* edge of the gate. Thus a gate can start the circuitry along the path to "hang up".

LeCroy has published an application note (AN-19) addressing a nuance of the problem: the possibility of partial gates by CLEAR coinciding with a legitimate gate. LeCroy later decided that the patch described in AN-19 did *not* solve the problem, and suggested an alternate. Their alternate patch did not fix it either.

LeCroy's position on the matter, as detailed in AN-19 and over the telephone, is that the 2249 (and 2259) were designed for synchronous operation, with no gates appearing during the readout/clear cycle. A true "fix" would require a complete redesign of the modules, and is not planned. People in our circumstances are expected to externally block gates during the internal clear cycle. This is made a little difficult since the signal which causes the problem is not available externally. We can program the MBD-11 to assert another output line prior to the MBD-11 issuing the CAMAC Clear command. External electronics can then block gates during that period. We have not tried this approach yet.

13. BOOSTER LINAC PROJECT

13.1 Introduction

D.W. Storm

The booster project was outlined in last year's Annual Report.[1] The overall layout is illustrated in Fig. 13.1. The only design change that has been made is the decision to use 24 low beta resonators followed by 12 high beta resonators, instead of using 12 of each, as originally planned. This change compensates for the fact that the optimum velocities of the resonators, as determined from field measurements, are about 10% higher than planned. Thus by using more low beta resonators, we obtain a profile of energy gain vs atomic mass that is very similar to the original plan.

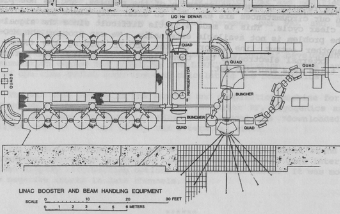

Fig. 13.1 Layout of the booster accelerator.

During the past year substantial progress has been made on the booster project. These efforts are discussed in some detail in the following sections. To summarize: the plating lab has been completed, commissioned, and has been used to plate a number of resonators. Several low beta resonators have been completed, plated, and tested successfully here at the Nuclear Physics Laboratory. A high beta prototype has been built, plated, and tested a number of times, but with limited success due to cracks or pits in an interior weld. Resonator controllers have been prototyped and several have been built. A satellite controller has been completed and tested with both high beta and low beta superconducting resonators.

Power and water for the accelerator are being installed. The refrigerator was completed and tested at 470 watts cooling (without nitrogen precool). This figure is substantially in excess of the specifications. The refrigerator is presently being installed here, along with the cryogen and helium gas storage vessels. Support structures for the accelerator cryostats have been delivered. The cryostats and cryogen distribution system are under construction. Contracts for most of the magnets have been placed. The low energy buncher has been built and is being tuned up. Reasonably detailed beam transport calculations have been carried out. The high voltage injection deck is being designed and specifications for the components are being prepared.

Eight staff members have been added (and two have left). The new staff members include two visiting scientists from Peking University. In addition to them, there are three new physicists, a plating technician, an electronic technician, and an instrument maker.

Reference:

1. Nuclear Physics Laboratory Annual Report, University of Washington (1984) Sec. 13.

******

13.2 Building Modifications

C.E. Linder and W.G. Weitkamp

Installation of the booster requires several modifications to the the Laboratory building. These fall into four categories: electrical, cooling water, air conditioning and shielding.

a. Electrical. The building is served by three-phase power at two voltages, 208 V and 460 V. Each voltage is supplied through a 500 kVA transformer. The existing load on the 208 V system is 100 kVA. The booster will add 203 kVA and the new polarized ion source 57 kVA. The total, 360 kVA, is well within the capacity of the transformer. However, the existing load on the 460 V system is 322 kVA (with the old polarized source removed). The booster will add 423 kVA. Most of this new load drives the helium refrigerator compressors. To cope with the total 745 kVA load, the old transformer will be replaced by a 1000 kVA transformer, which will allow some room for future expansion, but will fit in the available space. Four new circuit breaker panels will also to added to make power accessible to the booster.

b. Cooling. All of the electrical energy dissipated by the booster must be removed from the accelerator vault, mostly by water cooling power supplies. The tandem accelerator has an existing cooling water system, but the load from the booster would overwhelm it. Furthermore, the existing cooling tower is of the open circuit type, which permits the cooling water to make contact with air and to collect dirt and organic material. This has led to problems with pipe corrosion. Consequently, a new system with a closed circuit cooling tower will be installed, with provisions for maintaining the water at a high resistivity to minimize corrosion and stray currents.

c. Air conditioning. Not all the heat dissipated by the booster can be extracted by cooling water. We expect approximately 45 kW of power to be dissipated in the air of the accelerator vault. It not feasible to increase the capacity of the existing air conditioning system. To solve the heat problem, fan-coil units will be hung along the walls of the vault, using chilled water from the building refrigeration system, which has some spare capacity, to cool the air over the pumps, compressors and RF amplifiers, where most of the heat will be produced.

A consultant, Elcon Associates, has designed electrical, cooling water and air conditioning systems to meet the needs of the booster. Contractors are currently installing the equipment.

d. Shielding. In order to keep tandem accelerator based research going while the booster is being installed, it is desirable to shield the booster area from radiation produced by the accelerator. We have designed and installed a precast concrete block wall 3 ft thick by 7 ft high across the accelerator vault. Although this wall is not high or thick enough to shield against neutrons produced by beams of high energy protons or deuterons, it will permit personnel to work in the booster area during at least 80% of time the accelerator is operating.

******

13.3 Cryostat Supports

W.G. Weitkamp

The structures that support the cryostats on the booster must:

1. hold the cryostats rigidly, minimizing vibration,
2. permit easy alignment of the cryostats,
3. not create extraneous conducting paths for ground loop, and
4. be as economical as possible.

Steel and aluminum frameworks were considered, but precast reinforced concrete structures provide a nearly ideal solution to the problem. Concrete structures are rigid, non-magnetic and non-conductive if some care is taken to insulate reinforcing rods. Structures of concrete are significantly cheaper than those of steel or aluminum. Components can be grouted together if the forces are compressive or can be bolted together using connectors which are an integral part of the reinforcing if the forces are tensile.

Cryostats will set on a 3-sided concrete bases shaped like a fat letter "J" in plan view. The base structure is open to leave room for pumps and other auxiliary equipment attached to the cryostats. Wedge-type jack pads set on top of the bases will permit alignment of the cryostats. A plate of steel 3 in. thick will be bolted to I beams attached to one side of the base. This plate will shield personnel from x rays generated during resonator conditioning. Also attached to the I beams will be a catwalk to provide access to the tops of the cryostats and a tray to hold RF cables, control system cables, liquid helium distribution lines, etc.

******

13.4 Resonator Construction and Testing

J.F. Amsbaugh, M.A. Howe, and D.W. Storm

In last year's Annual Report[1] we described the successful construction and testing of the prototype low beta resonator at Stony Brook. Since then we have completed and equipped our own test facility, which includes cryostat and cryogen transfer equipment as well as RF power and test equipment. We have also begun production of the low beta resonators. Furthermore, we have built a prototype high beta resonator and have plated and tested it several times.

We have changed the construction technique for the low beta resonator slightly. The center conductor, center drift tube, and shorting plate are now all made from a single OFHC copper forging, instead of making them from three different pieces and welding them together. Otherwise the resonator is made the same as described in last year's Annual Report. We have built six low beta resonators and are presently in the process of building nine more. We have plated two of the ones made with the new technique and tested them.

The tests are carried out using the technique described in Ref. 1. From these tests we obtain curves of Q vs ‹E›, (where ‹E› is the average accelerating field, as defined in Ref. 1) which are shown in Fig. 13.4-1. The rapid fall off of the curves at high field is correlated with the appearance of x rays. The x-ray flux increases very rapidly with increasing field, as the Q curve falls. Therefore we attribute this fall off to the onset of field emission. The curves typically fall at about 1 MV/m in a newly plated resonator. The curves shown have been obtained after a conditioning process which involves operating at high power followed by pulsing with even higher power in the presence of 1×10^{-5} Torr of helium. During these treatments, as the Q fall off moves to higher fields, the field at which x-ray emission begins also increases. Although the resonators we have tested have low field Q values that are about half of those of the resonator tested at Stony Brook, the maximum attainable fields are actually higher. For both resonators, fields in excess of 3 MV/m are attainable with 6 watts of RF power being consumed in the resonator.

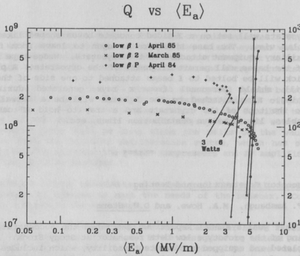

Fig. 13.4-1 Q plotted vs the average accelerating field for some low beta resonators. X-ray fluxes measured a foot from the cryostat are also plotted on the nearly vertical lines. The diagonal lines show Q vs field at two values of constant power.

We completed the design and built a prototype of the high beta resonator. It is illustrated in Fig. 13.4-2. This resonator has an inside diameter of 36 cm, twice the diameter of the low beta resonator. The optimum velocity for acceleration is 0.2 c. The length is about the same as that of the low beta resonator, although the center conductor is a few cm shorter and the gap between the end of the center conductor and the bottom plate is correspondingly larger. The features of the design have been presented elsewhere.[2,3] Basically, we scaled up the radial dimensions of the low beta resonator by a factor of two, but also increased the diameter of the drift tubes by more then a factor of two, and the curvature has been reduced to reduce surface fields for a given average accelerating field.

We have tested the resonator several times, but have not had a satisfactory result. Several pits or cracks in the interior weld between the shorting plate and the outer conductor have caused etched spots in the plated lead surface. When such spots were present, low-field Q's were poor. We tried to patch the spots with an indium-silver solder. When small amounts of the solder were used the patches cracked. When large amounts were used we found that we were able to cover the pits or cracks and get a good low-field Q (4×10^8). However, at moderate fields the Q would suddenly drop, as if some macroscopic region was going normal. We hypothesized that the solder patches were not conducting the heat from the lead surface, and that the whole patch surface was going normal. We are in the process of rebuilding the prototype resonator as well as procuring materials to make a second one.

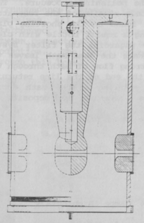

Fig. 13.4-2 High beta resonator.

References:

1. Nuclear Physics Laboratory Annual Report, University of Washington (1984) p. 94.
2. D.W. Storm, I. Ben-Zvi, and J.M. Brennan, Workshop on RF Superconductivity, Cern, Switzerland, 1984.
3. D.W. Storm, J.M. Brennan, and I. Ben-Zvi, 1985 Particle Accelerator Conference, Vancouver, BC, Canada, 1985.

*****

13.5 Plating

D.T. Corcoran

In October, 1984, the lead plating laboratory became operational.[1] Since then, five different resonators have been plated a total of fifteen times. The high beta resonator described in Sec. 13.4 was the first to be plated. Three different low beta resonators were plated with good test results on two of them. Finally, a rebuilt high beta resonator was plated. With this experience, we find that we are now able to obtain a smooth and shiny plated finish more than half of the times we plate.

During the many plating jobs, the normal plating and polishing procedures were refined and modified.[2] The most important modification was to not filter the lead bath with the addition agent in it for more than a few hours. It was found that the five micron filter did remove the additive over a period of time resulting in a poor surface finish. The second change was the use of a double rinse of acetone during the polishing procedure. This helped reduce the staining and gave a more thorough rinsing of the resonator. It was found that the crystals that are often found on the shorting plate could be washed out through the drain hole using a squirt bottle with clean acetone. Finally, two modifications were made regarding the filter system used during plating. First, the coupler plug where the lead bath leaves the resonator was modified so that there is not a strong flow of bath through the coupler hole. And second, an elbow was put at the end of the line returning the lead bath to the resonator to produce a swirling of the bath during plating. This added agitation also helps produce a smoother lead deposit.

The abbreviated plating/polishing procedure is as follows:

a) polish the resonator to a 2μ finish
b) wash with Micro
c) soak in Contrad (30 min.)
d) soak in 0.5% citric acid (30 min.)
e) pour in lead bath
f) put in anode, start filter, start heating
g) plate 12 hours at 2.6 Amps (low beta) or 4.8 Amps (high beta)
h) pour in aged and filtered polish (90 sec.)
i) pour in chelate, 1/4 chelate, ammonium hydroxide, and acetone
j) pour in second rinse of acetone (new step)
k) dry with warm nitrogen gas
l) inspect for and wash out any crystals (new step)
m) store in vacuum or load into cryostat

References:

1. Nuclear Physics Laboratory Annual Report, University of Washington (1984) p. 101.
2. Nuclear Physics Laboratory Annual Report, University of Washington (1984) p. 93.

******

13.6 Prototype Satellite Control Station

J.M. LaCroix, R.E. Stowell, and H.E. Swanson

The major components comprising the satellite control station include a chassis to hold the resonator controller modules, a panel with buttons and indicators used for local control of the resonators, and a microcomputer with various I/O modules which interface to the rest of the hardware. Fig. 13.6 shows a typical hardware configuration for the satellite station. The computer consists of a Digital Equipment Corporation (DEC) Falcon single board CPU, and Q-bus interface modules to provide analog and digital signals for setting and monitoring the other satellite system components. Each resonator controller is allocated 4 channels of analog input (ADC's), 4 channels of analog output (DAC's), and some number of digital I/O lines for operating switches and monitoring status. Since there is not a one-to-one correspondence between these I/O modules and the resonator controllers themselves, all signal lines from the computer are routed through a system interconnect board. The board uses wirewrap connections to map the signals between connectors and thus modifications are easily made during any stage of production. The local control panel is also interfaced to the computer through this board.

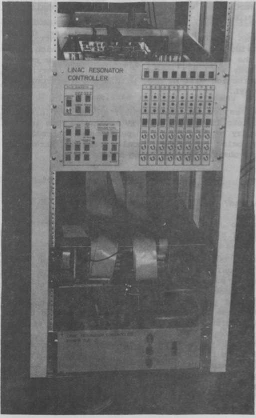

Fig. 13.6 The prototype linac satellite control station. The uppermost chassis contains the local control panel and resonator control modules. One of these is shown sitting on top with its cover removed. The DIGITAL Falcon based microcomputer is mounted below the control panel. Its front panel has been removed to show some of the cabling. The bottom unit is the power supply for the resonator controllers and associated electronics. The monitor used to display local parameters normally mounts in a shelf above the control panel, but is not shown here.

Local control functions are provided by the front panel. It is organized in three logical sections as follows: One section displays the status of individual resonators and permits the selection of any one of the resonator controllers for local control. There is LED indication that the controller board is powered up, indication that the amplitude and phase control loops are locked, and that the "Fast Out Of Lock" detect system is enabled for that resonator. The amplitude and phase control loop error signals for each resonator are available for observation at front panel BNC's as well as a sample of the RF picked off from the resonator itself. A second section permits the setting of parameters for the selected resonator. These include the overall loop phase, the phase difference between the phase locked resonator and the master oscillator, the input attenuation, and the position of the slow tuner and coupler stepping motors. The control loops may be turned on and off from this section as well. A third section contains the controls for the conditioning pulse generator.

Each satellite station can contain up to eight resonator controllers. The controllers, in their individual boxes, are mounted in a bin which holds them in good RF contact with the chassis and also allows them to be removed and placed a short distance away with all cables connected for service or diagnostic purposes. All construction will be done within the electronic and machine shop facilities at the NPL.

A video display module resides on the computer's bus and displays characters and numbers written into its memory on a TV monitor. This is used to provide a local status display of all resonator parameters controlled by the satellite. The resonator being controlled locally has its parameters shown in reverse video to better observe changes being made.

******

13.7 Satellite Control Software

L.W. Jackson, H.P. Readdy, R.J. Seymour, and H.E. Swanson

The multitasking software currently running in the Falcon based satellite controller was created using MicroPower Pascal and consists of an application program and kernel software, which provides basic support functions for the application program. The customized kernel, created from a set of software modules supplied by DEC and linked with the compiled application code, contains only those operating system services needed by the application. The application program, which is a static process, sets up concurrent dynamic processes in competition for use of the CPU and other system resources. Each concurrent process is designed to monitor and/or control a specific device such as a DRV11-J I/O board and can be blocked or unblocked by semaphores. These semiphores are controlled by events such as the system clock, device interrupts or other constraints and are used to synchronize the individual processes. A scheduler allows the unblocked process with highest priority to run. The Lab's VAX running VMS is used in development of the application program which is downloaded via a serial data link to a Falcon target where it is tested and debugged.

As an example, a system clock event sets a semaphore which then causes a process to run which monitors the resonator status lines and in addition, if a resonator is in local control, the status of control buttons and switches on the front panel. Increment-decrement buttons cause values output to DACs to be raised or lowered by an amount proportional to the length of time the button has been depressed. Parameters are changed in the appropriate data base, converted to the proper units, sent to the host, and displayed on the monitor. Stepping motor processes, activated by front panel buttons, change bit patterns which are then output through the DRV11J to motors that drive the resonator's coupler and tuner. Another process periodically reads each resonator's ADCs and updates an ADC data base which is examined for significant changes by update host and update screen processes. A host command parser waits for an input message from the host and upon receipt, calls the appropriate process to carry out the command.

An exception process intercepts error messages detected by the kernel, writes a message to the screen and does a hardware check before releasing the exception in an attempt to recover from it. A semaphore set by a loss of power in the satellite controller causes stepping motor processes and conditioning to halt in a predictable way. Restoration of power is followed by a message and a reset the front panel indication to its previous status.

******

13.8 Modifications to the Stony Brook Resonator Controller Board

J.M. LaCroix, H.E. Swanson, and L.P. Van Houten

After building and obtaining some operational experience with the resonator controller as obtained from S.U.N.Y. at Stony Brook, the following changes were made to increase its compatibility with other components in the satellite system. An additional stage of RF amplification was added between the reference phase shifter and the balanced mixer used to generate the phase error signal. This reduces the signal level requirement for the linac master clock. All digital control signals were made TTL compatible in order for them to be directly connected to the computer I/O modules. Analog error signals were routed to the edge connector on the circuit board and various traces on the outer perimeter of the board were modified to facilitate mounting in a commercially built components box made by MOD PAC, a division of Adams Russel Corporation. In the conditioning mode of operation, the resonators are pulsed on and off using a pulse generator common to all resonators controlled by the satellite. A conditioning mode switch was added to the board which permits an external DAC to set the quiescient power level when field stabilization is off. Printed circuit negatives were modified to include these and other changes. A few production units employing these modifications have been built and tested.

To facilitate building and testing 36 or more of these circuit boards, a procedure was developed for setting up all controller boards to the same initial conditions. In this procedure, the optimum settings of potentiometers which determine quiescent operating parameters of the board are found.

******

13.9 Main Control System

M.A. Howe and L.P. Van Houten

Significant progress has been made in the development of the booster main control program by using our computer (a VAX 11/780 with VMS) to get an early version of the program running now before the actual booster computer hardware (a MicroVAX with MicroVMS) becomes available. The software can trace its origins directly to the programs used to control the Stony Brook linac. The routines that we received from them were analyzed for function and the parts deemed useful were converted to run on our VAX. This has saved us considerable design and development time. All software to date is written in the C language and we anticipate little or no difficulty in converting the routines to run on the booster MicroVAX hardware since the VMS and MicroVMS operating systems are compatible.

The main control system's purpose is to provide a simple, easy to use, man-machine interface to the booster and to coordinate the activities of the numerous resonator control satellite computers. The software consists of four concurrently running processes:

1) The command interpreter. This routine monitors the master control terminal for commands, does the command parsing, and checks for proper command syntax.
2) The command dispatcher. This program serves as a clearing house for inter-process communication and handles all messages going to the satellite computers.
3) The satellite message interpreter. All messages coming from the satellites are received and interpreted by this routine. It also keeps a data base of all variables used in the satellites for resonator control.
4) The master display program. This program handles the real-time display of all system and satellite data base variables.

The system fully supports two-way communication between the host and any number of resonator control satellites. It is now being used to verify the operation of the satellite resident software and to explore various design concepts of the final main control program.

******

13.10 Cryogenic System

J.R. Cromie, D.J. Hodgkins, D.W. Storm, W.G. Weitkamp, and D.I. Will

The booster cryogenic system consists of the following items: a helium refrigerator, a cryogen distribution system, fourteen cryostats, and storage vessels for liquid nitrogen, liquid helium, and warm helium gas. A separate test cryostat is used for testing resonators individually.

The helium refrigerator as delivered is a Koch Process Systems[1] 2830S with 3 RS screw compressors as previously described[2] except as follows:

1) it has a pair of 2 inch diameter, 2 inch stroke, pistons in its wet engine,
2) the wet engine is equipped with a constant speed control which can both drive and brake to maintain engine speed, and
3) the refrigerator has a high conductance, plate-fin heat exchanger.

The refrigerator was tested at Koch in December, 1984. At 4.5 °K it delivered 470 watts cooling without liquid nitrogen precool and 610 watts cooling with liquid nitrogen precool. (The refrigerator will permit *in situ* upgrade to 1000 watts cooling capacity without liquid nitrogen, if necessary.) It will store all the boil-off gas from a 890 watt load without venting helium. It liquifies helium at 130 liters per hour. All these values exceed our specifications by comfortable margins. The refrigerator uses a 1000 liter Cryofab helium dewar with enlarged neck as a phase separator and liquid buffer. A 3000 cubic foot propane tank fabricated by Riley-Baeird serves as a warm helium gas buffer.

The cryogen distribution system consists of two parts. A standard vacuum-jacketed liquid nitrogen supply line runs from our 9000 gallon liquid nitrogen storage tank[3] to the helium refrigerator. A specially designed liquid helium/liquid nitrogen distribution system serves the cryostats from the refrigerator and dewar. This system carries liquid helium from the dewar to the cryostats and returns cold helium vapor to the refrigerator with minimum enthalpy gain. It also carries liquid nitrogen for cooling its own radiation shields and those in the cryostats. The nitrogen boil-off is not recovered. The system regulates cryogen flow to each cryostat via extended stem valves driven so as to maintain constant readings on the cryostat liquid level sensors. A particular innovation for this system is a demountable field joint designed to permit cryostat servicing, removal, and replacement without cutting or welding and without bayonet joints (which have proven to contribute large heat leaks at S.U.N.Y. Stony Brook[4]). These field joints use conflat fittings on all cryogen lines and have an O-ring sealed shell. They will be continuously pumped. The contract for the liquid helium/liquid nitrogen distribution system was awarded to Beech Aircraft, Boulder Division, April, 1985.

Ten out of an eventual fourteen cryostats of modified Weizmann Institute design[5] are currently under construction at Janis Research. Two are designed to hold single buncher resonators (either high or low beta.) The rest will hold either four low beta or two high beta resonators as needed.

The test cryostat was designed to hold a single resonator for radiofrequency power tests and conditioning. It has no beam ports, is lightweight, and rolls on rubber casters for easy transport from plating lab to test facility. It was delivered in October, 1984, by Beech Aircraft, Boulder Division, and quiescent liquid helium boil-off is consistent with the 1 liter/hour we specified. It has been used for seven resonator tests to date.

References:

1. Koch is the successor to CTI/Helix and Collins.
2. Nuclear Physics Laboratory Annual Report, University of Washington (1984) p. 101.
3. For economic reasons this MVE liquid nitrogen tank is sized to accept a full liquid nitrogen tanker truck load.
4. Heat leaks of 4 watts per male-female bayonet pair have been measured by Gene Sprouse at Stony Brook (discussion at SNEAP 1984).
5. Designed by Ilan Ben-Zvi, et al., Weizmann Institute of Science, Rehovot, Israel.

******

13.11 Vacuum System for the Booster Linac Project

J.F. Amsbaugh, D.W. Storm, and W.G. Weitkamp

The vacuum system for the booster linac project consists of the cooldown pumping and the beam transport pumping systems. The cooldown pumping system is used to provide a thermally insulating vacuum of low 10^{-6} Torr while the resonators are baked out and then cooled to cryogenic temperatures. This system is also used to pump He gas that is introduced during "He conditioning", while the resonators are at liquid He temperature. Each of the pumping systems consists of a turbomolecular pump (TMP), rated at 360 l/sec, backed by a 14-CFM direct-drive mechanical pump. Each system pumps on two cryostats and can be isolated by gate valves. The connection is made via a cross that also provides vibration and electrical isolation between the TMP and the cryostats. Electrical isolation is also provided by the beamline chambers between the cryostats to avoid ground loop problems, and after each cryostat there is an isolation gate valve in the beamline. All of this equipment has been acquired and was tested upon delivery.

The beam transport pumping system consists of two redesigned beamlines for the tandem and four new beamlines. The present object and image beamlines of the tandem will be converted to metal sealed systems and pumped by a TMP and cryopump; furthermore, a cryostat for the rebuncher-debuncher will be incorporated in the image beamline. Four new beamlines will be needed to connect the linac to the existing beam transport system (see Fig. 13.1). The dogleg beamline runs through several magnets that displace the beam from the tandem axis to the entrance axis of the linac. The dogleg will be pumped by ion pumps. The other new beamlines connect the entrance and exit of the linac to the image beamline. The last new beamline is in the 180° bend half way through the linac. These three beamlines will be pumped by TMPs. All of the pumping elements for these systems have been acquired and were tested upon delivery. The detailed design of the dogleg vacuum chambers are complete and soon to be under construction.

Conceptual design of the control system, considering the equipment acquired, has began and the detailed specifications should be completed soon.

******

13.12 Injector Deck

T.A. Trainor, L.P. Van Houten, and D.I. Will

The injector deck is a 300 kV platform supporting two ion sources (sputter source - 25 keV, and DEIS - 45 keV) with provision for a third installation. The injector was originally specified for 200 kV, but during the detailed design process it has become apparent that 300 kV is probably within our budget, and a higher injection energy significantly improves the linac beam quality for the heaviest ions.

The major elements are now specified. The deck itself will be manufactured by an outside vendor rather than within the NPL. The only notable feature is a cantilevered portion containing the ion sources themselves. This is required because of a step in the floor in the accelerator area, but has the additional desirable feature that ion sources can be serviced from the side in a standing posture with removal of a few light floor plates.

We have received word that a 300 kV power supply can be constructed with 10 volt P-P noise from available technology. This low noise figure is made possible by using a precision DC low voltage power supply to power the oscillator section of a standard RF-type high voltage supply and by using an additional filter stack in parallel with the Cockcroft-Walton stack on the supply output. Our original goal was 10-20 volts rms at 200 kV. Such a reduction in ion source noise transforms directly into improved energy-time beam quality.

AC power will be delivered to the deck via a 3-phase isolation transformer. Since the transformer technology is available this system is much preferred over the noise and maintenance requirements of an M-G set.

We have specified and found a supplier for a double-focussing 90° magnet consistent with the optical requirements of the deck layout and will use a type of acceleration tube which we have used with success previously on other ion source installations.

This list comprises all the long lead-time items on the project. The longest period is about nine months ARO. Other deck items, such as cooling, remote control and ion source installation are conventional and will be considered after these orders are placed.

******

13.13 Beam Dynamics

J.G. Cramer, J.-Q. Lu, and D.W. Storm

(a) Beam Transport Magnets. The beam transport magnets for the booster have been divided for the purposes of purchasing into four groups: (1) the dogleg elements consisting of four 45° dipoles and four quadrupole singlets, (2) the beam transport quadrupoles consisting of three quadrupole doublets, (3) the inter-cryostat quadrupoles consisting of 12 quadrupole doublets, and (4) the turnaround and final magnet elements consisting of three 90° dipoles and a quadrupole triplet. The group-1 magnets were put out for bid last year and were ordered from the Magnecoil Corp. of Boston on September 25, 1984, and are now being constructed. The group-2 magnets were bid early this year and the order was placed February 13, 1985 with Bruker, GMBH of West Germany. The group-3 magnets were put out for bid and the apparent low bidder is the Danfysik Corp. of Denmark. The order will be placed as soon as the DOE authorizes the foreign purchase. The group-4 magnets are now being specified and will be put out for bid in the near future.

(b) Beam Dynamics Calculations. The beam dynamics program LYRA written by A. Scholldorf of Stony Brook is being developed and improved to model and predict the performance of the booster. It transports a set of rays randomly distributed in a selected 6-dimensional phase space through a set of elements which model the accelerator. LYRA was modified last year[1] by expanding the array space and adding descriptions of the UW quarter-wave resonators.

This year we have made further modifications of Lyra which include: (1) Adding dipole magnets to the beam transport elements available; (2) Adding generalized transport elements describable by a 4×4 matrix; (3) Adding "dummy resonators" used for obtaining a snapshot of the beam at an arbitrary location; (4) Generalizing the phase space description to include "hollow" phase space tracing only the boundaries of the transported beam for more efficient calculations; and (5) Adding a "Pac-Man" phase space, equivalent to the "hollow" version except that there is a marker wedge which permits the observer to follow phase space rotations as the beam proceeds through the accelerator.

This modified version of LYRA has been checked with the program TRANSPORT, and gives identical predictions for dipole/quadrupole systems (with fringing field effects suppressed). A simulation has been performed demonstrating the transport of a deuterium beam through the model accelerator.

The program has now being further modified to include the effects of fringing fields in the dipole magnets, so that a more accurate modeling of the accelerator can be performed. These modifications are now being tested. Some attention is also be given to the possibilities for restructuring the code to reduce page-faulting and for adding search procedures similar to those available in TRANSPORT.

Reference:

1. "LYRA - A Beam Transport Program for Linear Accelerator with Independently Phased Non-Linear Resonators," A.H. Scholldorf, S.U.N.Y. Stony Brook, unpublished, 1983.

******

13.14 The Pretandem Buncher

J.F. Amsbaugh, J.G. Cramer, Q.-X. Lin, L. Sima, D.W. Storm, and T.D. Van Wechel

The control system for the pretandem buncher was designed last spring. The design is similar to the design of the Argonne National Laboratory.[1] The fundamental buncher frequency of 50 MHz and the first three harmonics are generated and phase locked to the 150 MHz linac clock frequency. Three of four independent control loops provide amplitude and phase control relative to the fundamental to enable synthesis of the buncher waveform. The amplitude of the buncher waveform and its phase with respect to the linac clock are controlled by the fourth control loop.

A prototype control loop at 50 MHz was constructed and tested with a model resonant line. Phase noise was found to be less than 0.01 deg and the phase drift over a 36 hour period was 0.05 deg with the control loop closed. The phase drift was found to be temperature dependent at about 0.01 deg per ^{o}C. Most of the observed drift was due to temperature variations. Amplitude noise was less than 0.1% with drift of 0.12% in a 48 hour period.

The buncher has been designed[2] and constructed. The buncher grid structure is the same as the ANL design. The resonant lines were shortened to provide the slightly higher frequency of 50 MHz. The vacuum chamber was enlarged and all of the buncher components mounted on one 6 inch O.D. Conflat flange. This vacuum chamber was made of 304L stainless steel and then electroplated with silver to a thickness of 0.001 in.

Construction of the control system was completed in December, 1984 and the construction of the buncher was completed in March, 1985. It has been assembled and bench testing is underway. Tests indicate that resonant lines need to be shortened further since the grid capacitance is larger than expected. Another problem that is being investigated is that the 3/4 λ harmonic is loaded differently than the 1/4 λ harmonic by the grid capacitance.

References:

1. F.J. Lynch, R.N. Lewis, L.M. Bollinger, W. Henning, and O.D. Despe, Nucl. Instrum. Methods 159, 245 (1979).
2. Nuclear Physics Laboratory Annual Report, University of Washington (1984) p. 96.

******

13.15 Beam Diagnostics

J.F. Amsbaugh, R.C. Connolly, and W.G. Weitkamp

Tuning the beam through the booster and diagnosing problems requires beam diagnostic instrumentation. We are planning to install seven types of devices on the booster: beam profile monitors, slits, Faraday cups, beam energy monitors, resonant phase detectors, time structure monitors, and emittance measuring devices.

We have prepared a plan for the layout of these devices, concentrating on the region of the dogleg magnets, which will be the first to be completed, and where space is most constricted. Both beam profile monitors and slits will be required in this area. We have selected the rotating helix type of beam profile monitor to use on the booster, because of the compact size of the units, simplicity of the readout system, and relatively wide acceptance of this type of unit at other labs. The design of a custom made, remotely operable slit which will fit into the space between the magnets of the dogleg has been completed.

14. APPENDIX

14.1 Nuclear Physics Laboratory Personnel

Faculty

Eric G. Adelberger, Professor
David Bodansky, Professor
John G. Cramer, Professor; Director, Nuclear Physics Laboratory
George W. Farwell, Professor
I. Halpern, Professor
Albert Lazzarini, Research Assistant Professor[1]
Eric Norman, Affiliate Assistant Professor[2]
Fred H. Schmidt, Professor
Kurt A. Snover, Research Professor
Thomas A. Trainor, Research Associate Professor
Robert Vandenbosch, Professor
William G. Weitkamp, Research Professor; Technical Director, Nuclear Physics Laboratory

Research Staff

Ilan Ben-Zvi, Visiting Scientist[3]
Cynthia A. Gossett, Research Associate
Qui-Xun Lin, Visiting Scientist[4]
Jian-Qin Lu, Visiting Scientist[5]
Tetsuya Murakami, Research Associate
Martin J. Murphy, Research Associate
John L. Osborne, Research Associate[6]
Christoph C. Sahm, Research Associate
Daniel R. Tieger, Research Associate

Senior Professional Staff

Harold Fauska, Senior Research Scientist[7]
Derek W. Storm, Senior Research Scientist

Predoctoral Research Associates

John A. Behr
Keith J. Davis
Gerald Feldman
Patricia Fernandez
Salvador Gil[8]
Jens Gundlach
David W. Holmgren[9]
Stephen Kellogg
Mahbubul A. Khandaker
Dat-Kwong Lock[10]
Robert A. Loveman[11]
Amlan Ray
Peter Wong
Valdis Zeps

Professional Staff

John F. Amsbaugh, Research Scientist
Roger Connolly, Reseach Engineer
Greg Douglas, Visiting Controls Engineer[12]
Thomas Goliak, Research Engineer[13]
Gervas M. Hinn, Research Scientist/Target Maker
David J. Hodgkins, Research Engineer
Mark A. Howe, Research Engineer
Donald D. Leach, Research Scientist
H. Pamela Readdy, Computer System Engineer
Alan G. Seamster, Research Scientist[14]
Richard J. Seymour, Computer System Manager
Rod E. Stowell, Electronics Engineer/Electronic Shop Supervisor
H. Erik Swanson, Research Physicist
Louis Van Houten, Research Engineer
Timothy Van Wechel, Electronics Engineer
Douglas I. Will, Research Engineer

Technical Staff

Robert L. Cooper, Instrument Maker
Dean T. Corcoran, Engineering Technician
James R. Cromie, Accelerator Technician
Ronald W. Floyd, Buyer
Louis Geissel, Instrument Maker, Student Shop Leadman
Brian P. Holm, Instrument Maker
John M. LaCroix, Electronics Technician
Carl E. Linder, Engineering Technician
George Saling, Accelerator Technician[7]
Lawrence Sima, Drafting Technician
Hendrik Simons, Instrument Maker, Shop Supervisor
Allen L. Willman, Instrument Maker[7]

Administrative Staff

Barbara J. Fulton, Administrative Secretary
Margaret M. Nims. Office Assistant
Maria G. Ramirez, Program Assistant

Part Time Staff

Darrell Armstrong
David Badt
Frederick Bahr
David Balsley
David Chan
Cindy Christensen[15]
Ky Clifford[15]
Jim Davis
Mark DeFaccio[15]
Tony Diego
Jane Fuller
Albert Herron
Norman Hill
Steven Holmes[15]
Lee Jackson
Peter James
Donna Kubik[15]
Kevin McMurry
Thomas Meadows
Eric Muller

David Newell
Quan Ngo[15]
Joseph Olson
David Patterson
Paul Perry[15]
Barbara Sanborn
Paul Viren[15]
Michael Walker[15]
Fawn Willis[15]
Eugene Wong

---

1. Now at: Kaman Instrumentation, Colorado Springs, CO 80933.
2. Now at: Lawrence Berkeley Laboratory, University of California, Berkeley, CA 94720.
3. Permanent Address: Department of Nuclear Physics, Weizmann Institute of Science Rehovot, Israel.
4. Permanent Address: Peking University, Peijing, People's Republic of China.
5. Permanent Address: Peking University, Peijing, People's Republic of China.
6. Deceased March 21, 1985.
7. Retired - part time employee.
8. Completed Ph.D. degree. Present Address: Comision Nacional de Energia Atomica, Av. del Libertador, 8250 Buenos Aires, Argentina.
9. Completed Ph.D. degree. Present Address: Kaman Sciences, Colorado Springs, CO 80933.
10. Completed Ph.D. degree. Present Address: 1033 Bayview Avenue, Oakland, CA 94610.
11. Completed Ph.D. degree. Present Address: University of Colorado, Boulder, CO 80309.
12. Permanent Address: Group 3 Technology Ltd., Auckland, New Zealand.
13. Now at Jet Propulsion Laboratory, California Institute of Technology, Pasadena, CA 91109.
14. Now at John Fluke Co., Everett, WA 98206.
15. No longer associated with the Nuclear Physics Laboratory.

******

14.2 Ph.D. Degrees Granted, Academic Year 1984-1985

Salvador Gil - Spin Distribution of the Compound Nucleus in Heavy Ion Reactions at Near-Barrier Energies

David Holmgren - A Search for Parity in Hydrogen and Deuterium

Robert Loveman - The Determination of the Total Reaction Cross Section for Heavy Ions at 15 MeV/AMU, 25 MeV/AMU, and 35 MeV/AMU

******

14.3 List of Publications

Published Papers

"On the Half-Life of ^{180}Ta in Stellar Environments," E.B. Norman, S.E. Kellogg, T. Bertram, S. Gil, and P. Wong, Astrophys. J. 281, 360 (1984).

"Equilibration of $^{176}Lu^{g,m}$ during the s-process," E.B. Norman, T. Bertram, S.E. Kelogg, S. Gil, and P. Wong, Astrophys. J. 291, 834 (1985).

"Giant Dipole Resonances Built on Highly Excited States of Light Nuclei," K.A. Snover, Comments on Nucl. Part. Phys. 12, 243 (1984).

"Production of Thick Elemental Low-Oxygen Content ^{nat,26}Mg from ^{nat,26}MgO," G.M. Hinn, E.B. Norman, T.E. Chupp, and K.T. Lesko, Nucl. Instrum. Methods 227, 434 (1984).

"The Accelerator Mass Spectrometry Facility at the University of Washington: Current Status and an Application to the ^{14}C Profile of a Tree Ring," G.W. Farwell, P.M. Grootes, D.D. Leach, and F.H. Schmidt, Nucl. Instrum. Methods B5, 144 (1984).

"Parity Mixing of Elastic Scattering Resonances: General Theory and Application to ^{14}N," E.G. Adelberger, P. Hoodbhoy, and B.A. Brown, Phys. Rev. C 30, 456 (1984).

"^{22}Na Production Cross Sections from the $^{19}F(\alpha,n)$ Reaction," E.B. Norman, T.E. Chupp, K.T. Lesko, P.J. Grant, and G.L. Woodruff, Phys. Rev. C 30, 1339 (1984).

"Transport and Evaporation Model Calculations of N and Z Distributions for Damped Nuclear Reactions," D.-K. Lock, R. Vandenbosch and J. Randrup, Phys. Rev. C 31, 1268 (1985).

"Observation of the Beta-Decay of $^{180}Hf^{m}$," S.E. Kellogg and E.B. Norman, Phys. Rev. C 31, 1505 (1985).

"Entrance Channel Dependence of Back Angle Yields: Orbiting in $^{24}Mg+^{16}O$ Reaction," A. Ray, S. Gil, M. Khandaker, D.D. Leach, D.-K. Lock, and R. Vandenbosch, Phys. Rev. C 31, 1573 (1985).

"Spin Distribution of the Compound Nucleus in Heavy Ion Reactions at Near-barrier Energies," S. Gil, R. Vandenbosch, A.J. Lazzarini, D.-K. Lock and A. Ray, Phys. Rev. C 31, 1753 (1985).

"Non-Equilibrium Excitation Energy Division in Deeply-Inelastic Collisions," R. Vandenbosch, A. Lazzarini, D. Leach, D.-K. Lock, A. Ray, and A. Seamster, Phys. Rev. Lett. 52, 1964 (1984).

"Determination of a Time Scale for the Emission of Energetic Photons in Heavy Ion Fusion Reactions," A. Lazzarini, V. Metag, D. Habs, W. Hernerici, J. Schmmer, Phys. Rev. Lett. 53, 1045 (1984).

"Comment on Fission Fragment Angular Distributions," R. Vandenbosch, Phys. Rev. Lett. 53, 1504 (1984).

"The Time Scale for Projectile Breakup into Coincident Heavy Fragments," M.J. Murphy, T.C. Awes, S. Gil, M.N. Harakeh, A. Ray, A.G. Seamster, and R. Vandenbosch, Phys. Rev. Lett. 53, 1543 (1984).

"Deformation of Heated Nuclei Observed in the Statistical Decay of the Giant Dipole Resonance," C.A. Gossett, K.A. Snover, J.A. Behr, G. Feldman, and J.L. Osborne, Phys. Rev. Lett. 54, 1486 (1985).

"Searches for Double β^+, β^+/EC and Double EC Decays," E.B. Norman and M.A. DeFaccio, Phys. Lett. B 148, 31 (1984).

"Symmetry Violation in Nuclei," E.G. Adelberger, Intersections between Particle and Nuclear Physics, edited by R.E. Mischke, AIP Conf. Proc. No. 128, (AIP, New York, 1984) p. 300.

"Some Methods and Problems Associated with Making Thick (1 Mg/cm^2) ^{28,29,30}Silicon Targets," G.M. Hinn, Proceedings of Workshop 1983 of the International Nuclear Target Development Society, ANL/PHY-84-2, edited by G. Thomas (Argonne National Laboratory 1984), p. 89.

"The Conceptual Design of the University of Washington Superconducting Booster," W.G. Weitkamp, Proceedings of the Symposium of Northeastern Accelerator Personnel, Edited by T. Lund (University of Rochester, 1983), p. 287.

"Studies of Symmetries in Nuclear Reactions," E.G. Adelberger, Proceedings of the INS-Riken International Symposium on Heavy Ion Physics, Part 1, J. Phys. Soc. Jpn 54, 6 (1985), Suppl. 1.

"Giant Resonances Built on Excited States," K.A. Snover, Proceedings of the International Symposium on Highly Excited States and Nuclear Structure," Editions de Physique C4, 337 (1984).

"High Energy Gamma Rays from Complex Particle Collisions," K.A. Snover, Proceedings of the 5th International Symposium on Capture Gamma Ray Spectroscopy, AIP Conf. Proc. No. 125 (AIP, New York, 1985), p. 660.

Papers Submitted or in Press

"The Parity Non-Conserving Nucleon-Nucleon Interaction," E.G. Adelberger and W.C. Haxton, Ann. Rev. of Nucl. and Part. Science, to be published.

"A Simple Production Method for Making 3 $\mu g/cm^2$ Cracked Slacked Carbon Accelerator Stripper Foils," G.M. Hinn, 12th World Conference of the INTDS, Antwerp, Belgium, 1984 (invited paper); Nucl. Instrum. Methods 237A, to be published.

"Nuclide Distributions for Fe-like Fragments in the $^{136}Xe + ^{56}Fe$ Reaction," D.K. Lock, R. Vandenbosch, K.T. Lesko, S. Gil, A.G. Seamster, D.D. Leach, and A.G. Lazzarini, Nucl. Phys., in press.

"Neutron Yields from Alpha-Particle Induced Reactions of Importance to Reactors," P.J. Grant, E.B. Norman, G.L. Woodruff, D.L. Johnson, T.E. Chupp, and K.T. Lesko, submitted to Nucl. Sci. Eng.

"Observation of Enhanced Transparency in Nucleus-Nucleus Total Reaction Cross Sections," R.A. Loveman, J.G. Cramer, D.D. Leach, A.J. Lazzarini, W.G. Lynch, M.-Y. Tsang, and J. Van der Plicht, submitted to Phys. Rev. C.

"Low Energy π^+ Inelastic Scattering from Nuclei to the Continuum," K.A. Aniol, D.T. Chiang, K.G.R. Doss, I. Halpern, M. Khandaker, D.W. Storm, D.R. Tieger, P.D. Barnes, B. Bassalleck, N.J. Colella, S.A. Dytman, R.A. Eisenstein, R. Grace, C. Maher, D. Marlow, P. Pile, F. Takeutchi, W.R. Wharton, J.F. Amann, J. Julien, submitted to Phy. Rev. C.

"Refractive Contributions in the Interaction of $^{12,13}C$ at 20 MeV/N," H.G. Bohlen, X.S. Chen, J.G. Cramer, P. Fröbrich, B. Gebauer, H. Lettau, A. Miczaika, W. von Oertzen, R. Ulrich, and T. Wilpert, submitted to Z. Phys. A.

"Giant Resonances Built on Highly Excited States," K.A. Snover, Proceedings of XV International Summer School in Nuclear Physics, Mikolajki, Poland, September 1983, to be published.

Conference Presentations and Abstracts

"Observation of the β-decay of $^{180}Hf^m$ to ^{180}Ta," S.E. Kellogg and E.B. Norman, Bull. Am. Phys. Soc. 29, 1048 (1984).

"Pre-equilibrium Neutron Emission from Transfer to Unbound States in Heavy Ion Reactions," R. Vandenbosch, Bull. Am. Phys. Soc. 30, 733 (1985).

"Parity and Time Reversal Violation in Nuclear Eigenstates," E.G. Adelberger, Bull. Am. Phys. Soc. 30, 738 (1985). (Bonner Prize Winner Lecture.)

"Projectile Breakup into Multiple Heavy Fragments," M.J. Murphy, T. Awes, S. Gil, M. Harakeh, D. Leach, A. Ray, A. Seamster, and R. Vandenbosch, Bull. Am. Phys. Soc. 30, 747 (1985).

"Deformation of Heated Nuclei," C.A. Gossett, K.A. Snover, J.A. Behr, G. Feldman, J.H. Gundlach, T. Murakami, and J.L. Osborne, Bull. Am. Phys. Soc. 30, 761 (1985).

"The 0^+; 0^- I=1 Doublet in ^{14}N," P.B. Fernandez, C.A. Gossett, J.L. Osborne, V.J. Zeps, and E.G. Adelberger, Bull. Am. Phys. Soc. 30, (1985).

"Does the Cabibbo Angle Vanish in Fermi Matrix Elements of High J States?" E.G. Adelberger, P.B. Fernandez, and J.L. Osborne, Bull. Am. Phys. Soc. 30, (1985).

"Spin Distribution in Heavy Ion Fusion at and Below the Coulomb Barrier," A. Lazzarini, International Conference on Fusion Reactions below the Coulomb Barrier, Cambridge, MA, June, 1984.

"Tests of Beta=0.1 and Development of Beta=0.2 Lead Plated Quarter Wave Resonator," D.W. Storm, I. Ben-Zvi, and J.M. Brennan, Workshop on RF Superconductivity, Cern, Switzerland, July, 1984.

"How is the Excitation Energy Divided in Partially Damped Collisions?" R. Vandenbosch, A. Lazzarini, D. Leach, D.-K. Lock, A. Ray, and A.G. Seamster, INS-Riken International Symposium on Heavy Ion Physics, Tokyo, Japan, August 1984.

"Breakup of Projectiles into Multiple Heavy Fragments," M.J. Murphy, S. Gil, M.N. Harakeh, A. Ray, A.G. Seamster, and R. Vandenbosch, *ibid.*

"Summary," R. Vandenbosch, Tsukuba International Symposium on Heavy-Ion Fusion Reactions, Tsukuba, Japan, September 1984, (invited talk).

"Statistical Decay of Giant Resonances," C.A. Gossett, Fast Nucleon Capture Workshop, Chapel Hill, NC, September 1984 (invited talk).

"Nucleon Decay of the Giant Dipole Resonance," K.A. Snover *ibid* (invited talk).

"Some Effects of High Temperature and Density on Neutron-Capture Nucleosynthesis," E.B. Norman and S.E. Kellogg, 5th International Symposium on Capture Gamma-Ray Spectroscopy and Related Topics, Knoxville, TN, September 1984 (invited talk).

"University of Washington Nuclear Physics Laboratory Report to SNEAP 1984," C.E. Linder, Symposium of Northeastern Accelerator Personnel, Stony Brook NY, October, 1984.

"Lead Plating Facility at the University of Washington Nuclear Physics Laboratory," A.G. Seamster, D.W. Storm, and W.G. Weitkamp, *ibid.*

"Overview and Status of the University of Washington Nuclear Physics Lab Booster Project," D.W. Storm, *ibid.*

"Nuclear Physics Laboratory Satellite Control System," H.E Swanson, *ibid.*

"Pre-Tandem Beam Buncher Control Electronics," T. Van Wechel, *ibid.*

"Crogenic System for the University of Washington Superconducting Booster," D.I. Will, *ibid.*

"Results from a Bragg Curve Spectrometer," D.D. Leach, Conference on Instrumentation for Heavy-Ion Nuclear Research, Oak Ridge, TN, October 1984.

"Gamma-Ray Production Cross Sections for Alpha-Particle Induced Reactions on ^{19}F and ^{23}Na," E.B. Norman, T.E. Chupp, K.T. Lesko, P. Schwalbach, and M.A. DeFaccio, International Conference on Nuclear Data for Basic and Applied Science, Sante Fe, NM, May 1985.

"The Universiy of Washington Superconducting Booster Linac," D.W. Storm, J.G. Cramer, W.G. Weitkamp, H.E. Swanson, D.I. Will, J. Amsbaugh, and T.A. Trainor, 1985 Particle Accelerator Conference, Vancouver, B.C., May, 1985.

"Superconducting Resonators for the University of Washington Superconducting Booster Linac," D.W. Storm, J.M. Brennan, and I. Ben-Zvi, *ibid.*

"Giant Dipole Resonances in Highly Excited Nuclei," K.A. Snover, Niels Bohr Centenial Nuclear Structure Symposium, Copenhagen, May 1985.

Other Publications by Members of the Laboratory and Other Laboratory Research

"Inclusive Pion Single-Charge-Exchange Reactions," D. Ashery, D.F. Geesaman, R.J. Holt, H.E. Jackson, J.R. Specht, K.E. Stephenson, R.E. Segel, P. Zupranski, H.W. Baer, J.D. Bowman, M.D. Cooper, M. Leitch, A. Erel, J. Comuzzi, R.P. Redwine, and D.R. Tieger, Phys. Rev. C 30, 946 (1984).

"Measurement of the Reaction $^4He(\gamma,\pi^0)^4He$ for E_γ=290 MeV," D.R. Tieger, E.C. Booth, J.P. Miller, B.L. Roberts, J. Comuzzi, G.W. Dodson, S. Gilad, and R.P. Redwine, Phys. Rev. Lett. 53, 755 (1984).

"Strong Interaction Effects in High-Z Kaonic Atoms," F. O'Brien, E. Austin, J.P. Miller, B.L. Roberts, D.R. Tieger, M. Eckhause, J. Ginkel, P.P. Guss, D.W. Hertzog, D. Joyce, J.R. Kane, C. Kenney, J. Kraiman, W.C. Phillips, W.F. Vulcan, R.E. Welsh, R.J. Whyley, R.G. Winter, R.J. Powers, R.B. Sutton, G.W. Dodson, and A.R. Kunselman, Conference on Nuclear Physics, Surrey, England, March 1985.

"Precision Measurements of the Σ^- Mass and Magnetic Moment and the K^- Mass," J.P. Miller, E. Austin, F. O'Brien, B.L. Roberts, D.R. Tieger, M. Eckhause, J. Ginkel, P.P. Guss, D.W. Hertzog, D. Joyce, C. Kenney, J. Kraiman, J.R. Kane, W.C. Phillips, W.F. Vulcan, R.E. Welsh, R.J. Whyley, R.G. Winter, R.J. Powers, R.B. Sutton, G.W. Dodson, and A.R. Kunselman, Annual Meeting of the Division Particles and Fields of the Am. Phys. Soc., Santa Fe, NM, October 1984.

ROW 4: STORM, FELDMAN, JAMES, CORCORAN, LONGWILL, ARMSTRONG, AMSBAUGH, CONNOLLY, VAN WECHEL, SIMONS, SIMA, HALPERN, FARWELL, HOWE, GROOTES, FLOYD, BODANSKY, HODGKINS, DAVIS, VANDENBOSCH

ROW 3: GOSSETT, READDY, SEYMOUR, SAHM, LACROIX, MURAKAMI, SANBORN, FULTON, HINN, STOWELL, TIEGER, VAN HOUTEN, LU, WEITKAMP

ROW 2: GUNDLACH, MULLER, HOLM, KELLOGG, LINDER, CRAMER, SCHMIDT, SWANSON, WILL, TRAINOR, SNOVER, LIN, GEISSEL

ROW 1: KHANDAKER, ZEPS, BEHR, CROMIE, McMURRY, DIEGO, LEACH, RAY, BALSLEY, WONG, OLSON